

Beyond the Mean-Field: Structured Deep Gaussian Processes Improve the Predictive Uncertainties

Jakob Lindinger^{1,2}, David Reeb¹, Christoph Lippert², Barbara Rakitsch¹

¹Bosch Center for Artificial Intelligence, Robert-Bosch-Campus 1, 71272 Renningen, Germany

²Hasso Plattner Institute, Prof. Dr. Helmert Str. 2-3, 14482 Potsdam, Germany

Abstract

Deep Gaussian Processes learn probabilistic data representations for supervised learning by cascading multiple Gaussian Processes. While this model family promises flexible predictive distributions, exact inference is not tractable. Approximate inference techniques trade off the ability to closely resemble the posterior distribution against speed of convergence and computational efficiency.

We propose a novel Gaussian variational family that allows for retaining covariances between latent processes while achieving fast convergence by marginalising out all global latent variables. After providing a proof of how this marginalisation can be done for general covariances, we restrict them to the ones we empirically found to be most important in order to also achieve computational efficiency.

We provide an efficient implementation of our new approach and apply it to several regression benchmark datasets. We find that it yields more accurate predictive distributions, in particular for test data points that are distant from the training set.

1 Introduction

Gaussian Processes (GPs) provide a non-parametric framework for learning distributions over unknown functions from data [1]: As the posterior distribution can be computed in closed-form, they return well-calibrated uncertainty estimates, making them particularly useful in safety critical applications [2], Bayesian optimisation [3], or active learning [4]. However, the analytical tractability of GPs comes at the price of reduced flexibility: Standard kernel functions make strong assumptions

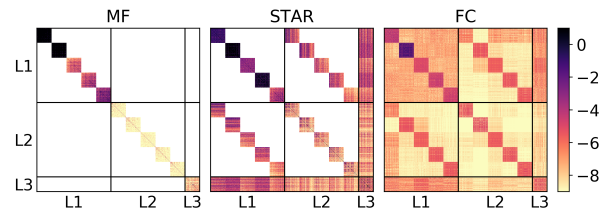


Figure 1: **Covariance matrices for variational posteriors.** We used a DGP with 2 hidden layers (L1 and L2) of 5 latent GPs each and increase the complexity of the variational approximation by allowing for additional dependencies within and across layers in a Gaussian variational family (left: mean-field, middle: stripes-and-arrow, right: fully-coupled). Plotted are natural logarithms of the absolute values of the variational covariance matrices over the inducing outputs.

such as stationarity or smoothness. To make GPs more flexible, a practitioner would have to come up with hand-crafted features or kernel functions, the latter resulting in additional hyperparameters. Both alternatives require expert knowledge and are prone to overfitting.

Deep Gaussian Processes (DGPs) offer a compelling alternative since they learn non-linear feature representations in a fully probabilistic manner via GP cascades [5]. This additional flexibility however means that inference can no longer be performed in closed-form, but must be approximated via Monte Carlo sampling [6], or deterministic approximations [5, 7, 8]. The most popular approximation, variational inference (VI), searches for the best approximate posterior within a pre-defined class of distributions: the variational family [9]. For GPs, variational approximations often build on the inducing point framework where a small set of global latent variables act as pseudo datapoints (x_M, f_M) that summarise the training data [10, 11]. For DGPs, each latent GP is governed by its own set of inducing variables, which, in general,

need not be independent from those of other latent GPs.

In this paper, we offer a new class of variational families for DGP models taking the following two requirements into account: (i) all global latent variables, i.e., inducing outputs f_M , can be marginalised out, (ii) correlations between latent GP models can be captured. Satisfying (i) reduces the variance in the estimators and is needed for fast convergence [12] while (ii) leads to better calibrated uncertainty estimates [13].

By using a fully-parameterised Gaussian variational posterior over the global latent variables, we automatically fulfil ii), and we show in Sec. 3.1, via a proof by induction, that i) can still be achieved. Our proof is constructive and results in a novel inference scheme for variational families that allows for correlations within and across layers. In Fig. 1 (right) we depict exemplary inferred covariances between the latent GP models. In addition to the diagonal blocks, the covariance matrix has visible diagonal stripes in the off-diagonal blocks and an arrow structure. These diagonal stripes point towards strong dependencies between successive latent GPs, while the arrow structure reflects dependencies between the output layer and all hidden layers. In Sec. 3.2, we further propose a scalable approximation to this variational family, which only takes these stronger correlations into account (Fig. 1, middle). We provide efficient implementations for both variational families, where we particularly exploit the sparsity and structure of the covariance matrix of the variational posterior.

In Sec. 4, we confirm experimentally that our new algorithm works well in practice, yielding accurate predictions and calibrated uncertainty estimates. The benefits of our approach are most prominent when the test points are distant from the training points as our method assigns larger and thereby more accurate uncertainties to distant test points. For safe AI applications there is an urgent need for calibrated uncertainties for distant test points [14]. Their occurrence can be a consequence of scarce training data, which is the underlying problem for Bayesian optimisation [3] and safe active learning [4], or unforeseen shifts in the data distributions that happen in many real-world applications [15].

2 Background

In the following, we introduce the notation that we use throughout the paper. Moreover, we provide the necessary background on DGP models. Sparse GPs are building blocks of DGP models and we start our review with these.

2.1 Sparse Gaussian Processes

In regression problems, the task is to learn a function $f : \mathbb{R}^D \rightarrow \mathbb{R}$ that maps a set of N input points $x_N = \{x_n\}_{n=1}^N$ to a corresponding set of noisy outputs $y_N = \{y_n\}_{n=1}^N$. Throughout this work, we assume iid noise, $p(y_N|f_N) = \prod_{n=1}^N p(y_n|f_n)$, where $f_n = f(x_n)$ and $f_N = \{f_n\}_{n=1}^N$ are the function values at the input points. We place a zero mean GP prior on the function f , $f \sim \mathcal{GP}(0, k)$, where $k : \mathbb{R}^D \times \mathbb{R}^D \rightarrow \mathbb{R}$ is the kernel function. This assumption leads to a multivariate Gaussian prior over the function values, $p(f_N) = \mathcal{N}(f_N|0, K_{NN})$ with covariance matrix $K_{NN} = \{k(x_n, x_{n'})\}_{n,n'=1}^N$.

In case of Gaussian likelihood, exact inference in this model is possible but incurs $\mathcal{O}(N^3)$ computational costs. Using sparse GPs, this limitation can be overcome [10, 11]: For this method a set of $M \ll N$ so-called inducing points $x_M = \{x_m\}_{m=1}^M$ from the input space is introduced. From the definition of a GP, the corresponding inducing outputs $f_M = \{f_m\}_{m=1}^M$, where $f_m = f(x_m)$, share a joint multivariate Gaussian distribution with f_N . We can therefore write the joint density of the model as

$$p(y_N, f_N, f_M) = p(f_N|f_M)p(f_M) \prod_{n=1}^N p(y_n|f_n), \quad (1)$$

where we factorised the joint prior into $p(f_M) = \mathcal{N}(f_M|0, K_{MM})$, the prior over the inducing outputs, and the conditional $p(f_N|f_M) = \mathcal{N}(f_N|\tilde{K}_{NM}f_M, \tilde{K}_{NN})$ with

$$\tilde{K}_{NM} = K_{NM}(K_{MM})^{-1}, \quad (2)$$

$$\tilde{K}_{NN} = K_{NN} - K_{NM}(K_{MM})^{-1}K_{MN}. \quad (3)$$

Here the matrices K are defined similarly as K_{NN} above, e.g. $K_{NM} = \{k(x_n, x_m)\}_{n,m=1}^{N,M}$.

Scalable inference in this model [Eq. (1)] can be achieved by employing VI: We search for an approximation $q(f_N, f_M)$ to the true posterior $p(f_N, f_M|y_N)$ by first choosing a variational family for the distribution q and then finding an optimal q that minimises the Kullback-Leibler (KL) divergence $\text{KL}[q||p]$. Equivalently, the so-called evidence lower bound (ELBO),

$$\mathcal{L} = \int q(f_N, f_M) \log \frac{p(y_N, f_N, f_M)}{q(f_N, f_M)} df_N df_M, \quad (4)$$

can be maximised. Following Refs. [11, 16], we choose the conventional variational family

$$q(f_N, f_M) = p(f_N|f_M)q(f_M), \quad (5)$$

¹Note that in our notation variables with an index m, M (n, N) denote quantities related to inducing (training) points. This implies for example that $x_{m=1}$ and $x_{n=1}$ are in general not the same.

where $q(f_M) = \mathcal{N}(f_M | \mu_M, S_M)$, and the mean μ_M and the covariance S_M are free variational parameters. The inducing outputs f_M act thereby as global latent variables that capture the information of the training data. Plugging (5) into (4), yields an ELBO of the form

$$\mathcal{L} = \sum_{n=1}^N \mathbb{E}_{q(f_n)} [\log p(y_n | f_n)] - \text{KL}[q(f_M) || p(f_M)], \quad (6)$$

where the $q(f_n)$ are the marginals of $q(f_N)$. The latter distribution is obtained by analytically marginalising out the inducing outputs f_M from the approximate posterior $q(f_N, f_M)$, resulting in $q(f_N) = \mathcal{N}(f_N | \tilde{\mu}_N, \tilde{\Sigma}_N)$, where

$$\begin{aligned} \tilde{\mu}_N &= \tilde{K}_{NM} \mu_M, \\ \tilde{\Sigma}_N &= K_{NN} - \tilde{K}_{NM} (K_{MM} - S_M) \tilde{K}_{NM}^\top. \end{aligned} \quad (7)$$

Variational parameters (μ_M, S_M) , model hyperparameters and the location of the inducing points x_M are obtained by maximising the ELBO (6). Since the latter decomposes over the data points, minibatch subsampling can be applied [16].

2.2 Deep Gaussian Processes

A deep Gaussian Process (DGP) is a hierarchical composition of GP models. We consider a model with L layers and T_l (stochastic) functions in layer $l = 1, \dots, L$, i.e., a total number of $T = \sum_{l=1}^L T_l$ functions [5]. The input of layer l is the output of the previous layer, $f_N^l = [f_N^{l,1}, \dots, f_N^{l,T_l}]$, with starting values $f_N^0 = x_N$. We place independent GP priors augmented with inducing points on all the functions, using the same kernel k^l and the same set of inducing points x_M^l within layer l . This leads to the following joint model density:

$$p(y_N, f_N, f_M) = p(y_N | f_N^L) \prod_{l=1}^L p(f_N^l | f_M^l; f_N^{l-1}) p(f_M^l). \quad (9)$$

Here $p(f_M^l) = \prod_{t=1}^{T_l} \mathcal{N}(f_M^{l,t} | 0, K_{MM}^l)$ and $p(f_N^l | f_M^l; f_N^{l-1}) = \prod_{t=1}^{T_l} \mathcal{N}(f_N^{l,t} | \tilde{K}_{NM}^l f_M^{l,t}, \tilde{K}_{NN}^l)$, where \tilde{K}_{NM}^l and \tilde{K}_{NN}^l are given by the equivalents of Eqs. (2) and (3), respectively.²

Inference in this model (9) is intractable since we cannot marginalise over the latents f_N^1, \dots, f_N^{L-1} as they act as inputs to the non-linear kernel function. We therefore

²In order to avoid pathologies created by highly non-injective mappings in the DGP [17], we follow Ref. [7] and add non-trainable linear mean terms given by the PCA mapping of the input data to the latent layers. Those terms are omitted from the notation for better readability.

choose to approximate the posterior by VI using the following variational family [7]:

$$q(f_N, f_M) = q(f_M) \prod_{l=1}^L p(f_N^l | f_M^l; f_N^{l-1}). \quad (10)$$

Note that $f_M = \{f_M^{l,t}\}_{l,t=1}^{L,T_l}$ contains the inducing outputs of all layers and might be covarying. This observation will be the starting point for our structured approximation in Sec. 3.1.

In the remaining part of this section, we follow the literature [7] and add a second restriction to the variational family by assuming that the inducing outputs are a-posteriori independent between different GPs (known as mean-field assumption, see also Fig. 1, left):

$$q(f_M) = \prod_{l=1}^L \prod_{t=1}^{T_l} q(f_M^{l,t}), \quad (11)$$

where $q(f_M^{l,t}) = \mathcal{N}(f_M^{l,t} | \mu_M^{l,t}, S_M^{l,t})$ and $\mu_M^{l,t}, S_M^{l,t}$ are free variational parameters. Plugging Eqs. (9) - (11) in Eq. (4), we can simplify the ELBO to

$$\mathcal{L} = \sum_{n=1}^N \mathbb{E}_{q(f_n^L)} [\log p(y_n | f_n^L)] - \sum_{l,t=1}^{L,T_l} \text{KL}[q(f_M^{l,t}) || p(f_M^{l,t})]. \quad (12)$$

We first note that this formula looks remarkably similar to the sparse GP case [Eq. (6)]. However, there is a subtle difference, namely that the marginals of the output of the last layer $q(f_n^L)$ cannot be obtained analytically. While the mean-field assumption renders it easy to analytically marginalise out the inducing outputs (see Appx. C.1), the outputs of the intermediate layers cannot be fully integrated out, since they are kernel inputs of the respective next layer, leaving us with

$$q(f_n^L) = \int \prod_{l=1}^L q(f_n^l; f_n^{l-1}) df_n^1 \dots df_n^{L-1}. \quad (13)$$

The terms appearing in Eq. (13) are all Gaussians,

$$q(f_n^l; f_n^{l-1}) = \prod_{t=1}^{T_l} \mathcal{N}(f_n^{l,t} | \tilde{\mu}_n^{l,t}, \tilde{\Sigma}_n^{l,t}), \quad (14)$$

where the means and covariances are given by the equivalents of Eqs. (7) and (8) (with $K^{l,t} = K^l \forall t$). We can therefore straightforwardly obtain samples from $q(f_n^L)$ by recursively sampling through the layers using Eq. (14). Those samples can be used to evaluate the ELBO [Eq. (12)] and we can additionally use the reparameterisation trick [12, 18] to obtain unbiased gradients for parameter optimisation. This stochastic estimator of

the ELBO has low variance as we only need to sample over the local latent parameters f_n^1, \dots, f_n^{L-1} , while we can marginalise out the global latent parameters, i.e. inducing outputs, f_M .

Finally, predictions can be made by taking multiple samples from $q(f_*^L)$ using Eq. (13), where the training input is being replaced by the test input x_* . The resulting predictive distribution is a mixture of Gaussians that can in principle approximate arbitrarily complex distributions.

3 Structured Deep Gaussian Processes

In this section, we introduce a new class of variational families that allows to couple the inducing outputs f_M within and across layers. Surprisingly, analytical marginalisation over the inducing outputs f_M is still possible, enabling an efficient inference scheme that refrains from sampling any global latent variables. Further speed-ups can be attained by focusing on the most prominent interactions, as we show in the second part.

3.1 Fully-Coupled DGPs

We present in the following a new variational family that strikes a good balance between efficient computations and expressivity: Our approach is efficient, since all global latent variables can be marginalised out, and expressive, since we allow for structure in the variational posterior. We do this by leaving the Gaussianity assumption made in Eq. (11) unchanged, while we introduce dependencies between all inducing outputs (within layers and also across layers). This leads to

$$q(f_M) = \mathcal{N}(f_M | \mu_M, S_M). \quad (15)$$

with dimensionality TM . In contrast to Eq. (11), our new family takes the dependencies between the latent processes into account, which makes the resulting variational posterior $q(f_N, f_M)$ in Eq. (10) better suited to closely approximate the true posterior. We give a comparison of exemplary covariance matrices S_M in Fig. 1.

Next, we investigate how the ELBO computations have to be adjusted when using the fully-coupled variational family. Plugging Eq. (15) into Eqs. (4), (9), (10), yields

$$\mathcal{L} = \sum_{n=1}^N \mathbb{E}_{q(f_n^L)} [\log p(y_n | f_n^L)] - \text{KL}[q(f_M) || \prod_{l=1}^L p(f_M^l)], \quad (16)$$

which we derive in detail in Appx. B. The major difference to the mean-field DGP lies in the marginals $q(f_n^L)$ of the outputs of the last layer. While the inducing outputs f_M could be rather straightforwardly marginalised out in the mean-field DGP (see Appx. C.1), this is no

longer the case for the fully-coupled DGP. Our findings about the implications of using a fully coupled $q(f_M)$ [Eq. (15)] are summarised in the following theorem:

Theorem 1. *In a fully-coupled DGP as defined above, for each data point x_n , the marginals $q(f_n^L)$ can be written as*

$$q(f_n^L) = \int \prod_{l=1}^L q(f_n^l | f_n^1, \dots, f_n^{l-1}) df_n^1 \dots df_n^{L-1}, \quad (17)$$

where all the distributions are conditionally Gaussian. They have the form

$$q(f_n^l | f_n^1, \dots, f_n^{l-1}) = \mathcal{N}\left(f_n^l \mid \hat{\mu}_n^l, \hat{\Sigma}_n^l\right), \quad (18)$$

where the means and covariances are given by

$$\hat{\mu}_n^l = \tilde{\mu}_n^l + \tilde{S}_n^{l,1:l-1} \left(\tilde{S}_n^{1:l-1,1:l-1}\right)^{-1} (f_n^{1:l-1} - \tilde{\mu}_n^{1:l-1}), \quad (19)$$

$$\hat{\Sigma}_n^l = \tilde{S}_n^{ll} - \tilde{S}_n^{l,1:l-1} \left(\tilde{S}_n^{1:l-1,1:l-1}\right)^{-1} \tilde{S}_n^{1:l-1,l}, \quad (20)$$

and $\tilde{\mu}_n^l$ and $\tilde{S}_n^{ll'}$ are defined as

$$\tilde{\mu}_n^l = \tilde{\mathcal{K}}_{nM}^l \mu_M^l, \quad (21)$$

$$\tilde{S}_n^{ll'} = \delta_{ll'} \mathcal{K}_{nn}^l - \tilde{\mathcal{K}}_{nM}^l \left(\delta_{ll'} \mathcal{K}_{MM}^l - S_M^{ll'}\right) \tilde{\mathcal{K}}_{Mn}^{l'}. \quad (22)$$

In Eqs. (19) and (20) the notation $A^{l,1:l'}$ is used to index a submatrix of the variable A , e.g. $A^{l,1:l'} = (A^{l,1} \dots A^{l,l'})$. Additionally, $\mu_M^l \in \mathbb{R}^{T_l M}$ denotes the subvector of μ_M that contains the means of the inducing outputs in layer l , and $S_M^{ll'} \in \mathbb{R}^{T_l M \times T_{l'} M}$ contains the covariances between the inducing outputs of layers l and l' . For Eqs. (21) and (22), we introduced the notation $\mathcal{K}^l = (\mathbb{I}_{T_l} \otimes K^l)$ as shorthand for the Kronecker product between the identity matrix \mathbb{I}_{T_l} and the covariance matrix K^l , and used δ for the Kronecker delta.

Before we proceed to provide a sketch of the proof of Thm. 1, we will first verify that Eq. (18) reduces to Eq. (14) when we plug in the mean-field posterior (11) in our formulas: In the notation of Eq. (15) this means restricting the covariance matrix to $S_M = \text{diag}(\{S_M^{ll}\}_{l=1}^L)$, where $S_M^{ll} = \text{diag}(\{S_M^{l,t}\}_{t=1}^{T_l})$ (see also Fig. 1, left).

Removing the correlations between the layers by setting $S_M = \text{diag}(\{S_M^{ll}\}_{l=1}^L)$, also implies that $\tilde{S}_n^{ll'} = 0$ if $l \neq l'$ [Eq. (22)]. Therefore Eqs. (19) and (20) reduce to $\hat{\mu}_n^l = \tilde{\mu}_n^l$ and $\hat{\Sigma}_n^l = \tilde{S}_n^{ll}$. The resulting variational posterior factorises between the layers with $q(f_n^l; f_n^{l-1}) = \mathcal{N}\left(f_n^l \mid \tilde{\mu}_n^l, \tilde{S}_n^{ll}\right)$.

Removing the correlations within one layer by setting $S_M^{ll} = \text{diag}(\{S_M^{l,t}\}_{t=1}^{T_l})$ renders the covariance matrix

\tilde{S}_n^l block-diagonal. The diagonal blocks are obtained by evaluating Eq. (22) with $S_M^l = \text{diag}(\{S_M^{l,t}\}_{t=1}^{T_l})$. It is easy to see that these diagonal blocks are equal to $\tilde{S}_n^{l,t}$ and we recover the mean-field solution [Eq. (14)].

By Thm. 1, the inducing outputs f_M can still be marginalised out, which enables low-variance estimators of the ELBO. While the resulting formula for $q(f_n^l | f_n^1, \dots, f_n^{l-1})$ has a similar form as Gaussian conditionals, this is only true at first glance: The latents of the preceding layers $f_n^{1:l-1}$ enter the mean $\hat{\mu}_n^l$ and the covariance matrix $\hat{\Sigma}_n^l$ also in an indirect way over \tilde{S}_n as they appear as inputs to the kernel matrices in Eq. (22).

Sketch of the proof of Theorem 1. We start the proof with the general formula for $q(f_n^L)$,

$$\int \left[\int q(f_M) \prod_{l'=1}^L p(f_n^{l'} | f_M^{l'}) df_M \right] df_n^1 \dots df_n^{L-1}, \quad (23)$$

which is already (implicitly) used in Ref. [7] and which we derive in Appx. C. In order to show the equivalence between the inner integral in Eq. (23) and the integrand in Eq. (17) we proceed to find a recursive formula for integrating out the inducing outputs layer after layer

$$\int q(f_M) \prod_{l'=1}^L p(f_n^{l'} | f_M^{l'}) df_M = \left[\prod_{l'=1}^{l-1} q(f_n^{l'} | f_n^{1:l'-1}) \right] \times \int q(f_n^l, f_M^{l+1:L} | f_n^{1:l-1}) \prod_{l'=l+1}^L p(f_n^{l'} | f_M^{l'}) df_M^{l'}. \quad (24)$$

The equation above holds for $l = 1, \dots, L$ after the inducing outputs of layers $1, \dots, l$ have already been marginalised out. This is stated more formally in Lem. 2 in Appx. A, in which we also provide exact formulas for all terms. Importantly, all of them are multivariate Gaussians with known mean and covariance.

The lemma itself can be proved by induction. While the terms appearing in this proof are rather lengthy, we will show the general idea of the induction step here: For this, we assume the right hand side of Eq. (24) to hold for some layer l and then prove that it also holds for $l \rightarrow l + 1$. We start by taking the (known) distribution within the integral and split it in two by conditioning on f_n^l :

$$q(f_n^l, f_M^{l+1:L} | f_n^{1:l-1}) = q(f_n^l | f_n^{1:l-1}) q(f_M^{l+1:L} | f_n^{1:l}). \quad (25)$$

Then we show that the distribution $q(f_n^l | f_n^{1:l-1})$ can be written as part of the product in front of the integral in Eq. (24) (thereby increasing the upper limit of the product to l). Next, we consider the integration over f_M^{l+1} , where we collect all relevant terms (thereby increasing

the lower limit of the product within the integral to $l+2$):

$$\begin{aligned} & \int q(f_M^{l+1:L} | f_n^{1:l}) p(f_n^{l+1} | f_M^{l+1}) df_M^{l+1} \\ &= \int q(f_M^{l+1} | f_n^{1:l}) q(f_M^{l+2:L} | f_n^{1:l}, f_M^{l+1}) p(f_n^{l+1} | f_M^{l+1}) df_M^{l+1} \\ &= \int q(f_M^{l+1} | f_n^{1:l}) q(f_n^{l+1}, f_M^{l+2:L} | f_n^{1:l}, f_M^{l+1}) df_M^{l+1} \\ &= q(f_n^{l+1}, f_M^{l+2:L} | f_n^{1:l}) \end{aligned} \quad (26)$$

The terms in the first line are given by Eqs. (25) and (9). All subsequent terms are also multivariate Gaussians that are obtained by standard operations like conditioning, joining two distributions, and marginalisation. We can therefore give an analytical expression of the term in Eq. (26), which is exactly the term that is needed on the right hand side of Eq. (24) for $l \rightarrow l + 1$. Confirming that this term has the correct mean and covariance completes the induction step.

After proving Lem. 2, Eq. (24) can be used. For the case $l = L$ the right hand side can be shown to yield $\prod_{l=1}^L q(f_n^l | f_n^1, \dots, f_n^{l-1})$. Hence, Eq. (17) follows by substituting the inner integral in Eq. (23) by this term. The full proof can be found in Appx. A. \square

We summarise the resulting algorithm for calculating the ELBO (16) in Algs. 1, 2, and 3. Alg. 1 shows how the ELBO can be calculated, where we average over multiple samples to reduce noise obtained by sampling through the layers. Alg. 2 zooms into a single layer of the DGP and differentiates the mean-field approach and ours: All coupled DGP approaches compute additional blocks of the covariance matrix \tilde{S}_n (marked in orange in Alg. 3) that lead to a dependency of the output of the current layer f_n^l on its predecessors $f_n^{1:l-1}$ (marked in orange).

In the following, we used our novel variational approach to fit a fully coupled DGP model with $L = 3$ layers to the *concrete* UCI dataset. We can clearly observe that this algorithmic work pays off: Fig. 1 shows that there is more structure in the covariance matrix S_M than the mean-field approximation allows. This is also reflected on the ELBO values for which we observe larger values for the fully-coupled DGP compared to the mean-field DGP ($\text{ELBO}_{FC} = -359$ vs. $\text{ELBO}_{MF} = -414$).

However, the increase in the number of variational parameters also leads to an increase in runtime and made convergence with standard optimisers fragile due to many local optima. While we could circumvent the latter by the use of natural gradients [19], which have been found to work well for (D)GP models before [3, 20, 21], the increased runtime need persists (see Sec. 4.2). It is therefore necessary to find a smaller variational family if

Algorithm 1 ELBO for coupled DGP

given minibatch x_{N_b}, y_{N_b} of size N_b , and number of Monte Carlo repetitions R

$\mathcal{L} = 0$

for $n = 1 \dots N_b$ **do**

list = $[x_n]$ \triangleright accumulates $\tilde{\mathcal{K}}_{nM}^l, \tilde{\mu}_n^l, \tilde{S}_n^{1:l,1:l}, f_n^l$

for $r = 1 \dots R$ **do**

for $l = 1 \dots L$ **do** \triangleright Alg. 2

$\hat{\mu}_n^l, \hat{\Sigma}_n^l, \text{list} = \text{sample_layer}(l, \text{list})$

$\mathcal{L} += \frac{N}{N_b S} \text{var_log_likelihood}(y_n, \hat{\mu}_n^L, \hat{\Sigma}_n^L)$

$\mathcal{L} -= \text{KL.term}()$

return \mathcal{L} \triangleright ELBO from Eq. (16)

Algorithm 2 `sample_layer(l, list)`: Return $\hat{\mu}_n^l, \hat{\Sigma}_n^l$ and sample f_n^l , update relevant quantities for later layers.

\triangleright list contains $\tilde{\mathcal{K}}_{nM}^{1:l-1}, \tilde{\mu}_n^{1:l-1}, \tilde{S}_n^{1:l-1,1:l-1}, f_n^{1:l-1}$

$\tilde{\mu}_n^l = \text{get_mu_tilde}()$ \triangleright Eq. (21)

$\tilde{S}_n^{l,1:l} = \text{get_S_tilde}(l, \tilde{\mathcal{K}}_{nM}^{1:l})$ \triangleright Alg. 3

$\hat{\mu}_n^l = \tilde{\mu}_n^l + \text{correct_mu}(\text{list}, \tilde{S}_n^{l,1:l-1})$ \triangleright Eq. (19)

$\hat{\Sigma}_n^l = \tilde{S}_n^{ll} - \text{correct_Sigma}(\text{list}, \tilde{S}_n^{l,1:l-1})$ \triangleright Eq. (20)

$f_n^l = \text{sample_multivariate_gauss}(\hat{\mu}_n^l, \hat{\Sigma}_n^l)$

list = `append`(list, $\tilde{\mathcal{K}}_{nM}^l, \tilde{\mu}_n^l, \tilde{S}_n^{l,1:l-1}, \tilde{S}_n^{ll}, f_n^l$)

return $\hat{\mu}_n^l, \hat{\Sigma}_n^l, \text{list}$ \triangleright Return to Alg. 1

Algorithm 3 `get_S_tilde(l, $\tilde{\mathcal{K}}_{nM}^{1:l}$)`: Calculate $\tilde{S}_n^{1:l,1:l}$ and $\tilde{S}_n^{l,l}$ according to Eq. (22) for the fully-coupled DGP.

$(S_M^{ll'})_{tt'}$ denotes the $M \times M$ block in S_M that contains the covariances of the inducing outputs of the t -th GP in the l -th layer and the t' -th GP in the l' -th layer. Analogously for $(\tilde{S}_n^{ll'})_{tt'}$.

for $l' = 1 \dots l$ **do**

for $t, t' = 1 \dots T_l, 1 \dots T_{l'}$ **do**

if $l = l'$ and $t = t'$ **then**

$(\tilde{S}_n^{l,l})_{tt} = \tilde{\mathcal{K}}_{nM}^l ((S_M^{ll})_{tt} - K_{MM}^l) \tilde{\mathcal{K}}_{Mn}^l$

$(\tilde{S}_n^{l,l})_{tt} += K_{nn}^l$

else

$(\tilde{S}_n^{l,l'})_{tt'} = \tilde{\mathcal{K}}_{nM}^l (S_M^{ll'})_{tt'} \tilde{\mathcal{K}}_{Mn}^{l'}$

return $\tilde{S}_n^{1:l,1:l}$ \triangleright Return to Alg. 2

we want to use the method in large-scale machine learning applications.

An optimal variational family combines the best of both worlds, i.e., being as efficient as the mean-field DGP while retaining the most important interactions introduced in the fully-coupled DGP. We want to emphasise that there are many possible ways of restricting the covariance matrix SM that potentially lead to benefits in

different applications. For example, Ref. [22] studies the compositional uncertainty in deep GPs using a particular restriction of the inverse covariance matrix. The authors also provide specialised algorithms to marginalise out the inducing outputs in their model. Here, we provide an analytic marginalisation scheme for arbitrarily structured covariance matrices that will vastly simplify future development of application-specific covariances. Through the general framework that we have developed, testing them is straightforward and can be done via simply implementing a naive version of the covariance matrix in our code.³ In the following, we propose one possible class of covariance matrices based on our empirical findings.

3.2 Stripes-and-Arrow Approximation

In this section, we describe a new variational family that balances efficiency and expressivity by sparsifying the covariance matrix S_M . Inspecting Fig. 1 (right) again, we observe that besides the $M \times M$ blocks on the diagonal, the diagonal stripes [25] (covariances between the GPs in latent layers at the same relative position), and an arrow structure (covariances from every intermediate layer GP to the output GP) receive large values. We therefore propose to keep only these terms and neglect all other dependencies by setting them to zero in the covariance matrix, resulting in a structure consisting of an arrowhead and diagonal stripes (see Fig. 1 middle). Note that this structure can only be employed if the same number of GPs in all the latent layers is used. But since this is the case for almost all reported results using DGPs [3, 6, 7], we do not see this as a major restriction.

Denoting the number of GPs per latent layer as τ , it is straightforward to show that the number of non-zero elements in the covariance matrices of mean-field DGP, stripes-and-arrow DGP, and fully-coupled DGP scale as $\mathcal{O}(\tau LM^2)$, $\mathcal{O}(\tau L^2 M^2)$, and $\mathcal{O}(\tau^2 L^2 M^2)$, respectively. In the example of Fig. 1, we have used $\tau = 5$, $L = 3$, and $M = 128$, yielding 1.8×10^5 , 5.1×10^5 , and 2.0×10^6 non-zero elements in the covariance matrices. While reducing the number of parameters already leads to shorter training times since less gradients need to be computed, we can furthermore exploit the structure of the covariance matrix for efficient computations.

The property that makes this form so compelling is that the covariance matrix $\tilde{S}_n^{1:l-1,1:l-1}$ [needed in Eqs. (19) and (20)] as well as the Cholesky decomposition⁴ of S_M

³Python code (building on GPflow [23] and TensorFlow [24]) implementing our method is provided at https://github.com/boschresearch/Structured_DGP.

⁴In order to ensure that S_M is positive definite, we will numerically only work with its Cholesky factor L , a unique lower

Algorithm 4 get. $\tilde{S}_n^{l,1:l}$: Calculate $\tilde{S}_n^{l,1:l-1}$ and $\tilde{S}_n^{l,l}$ for the stripes-and-arrow DGP.

```

for  $l' = 1 \dots l$  do
  for  $t, t' = 1 \dots T_l, 1 \dots T_{l'}$  do
    if  $l = l'$  and  $t = t'$  then
       $(\tilde{S}_n^{l,l})_{tt} = \tilde{K}_{nM}^l ((S_M^l)_{tt} - K_{MM}^l) \tilde{K}_{Mn}^l$ 
       $(\tilde{S}_n^{l,l})_{tt} += K_{nn}^l$ 
    else if  $l = L$  or  $t = t'$  then
       $(\tilde{S}_n^{l,l'})_{tt'} = \tilde{K}_{nM}^l (S_M^{l'})_{tt'} \tilde{K}_{Mn}^{l'}$ 
  return  $\tilde{S}_n^{l,1:l}$  ▷ Return to Alg. 2

```

have the same sparsity pattern. Therefore only the non-zero elements at pre-defined positions have to be calculated which is explained in Appx. D. This is also shown in Alg. 4, where we marked elements of $\tilde{S}_n^{l,1:l}$, that still need to be calculated, in orange.

The complexity for the ELBO is $\mathcal{O}(NM^2\tau L^2 + N\tau^3L^3 + M^3\tau L^3)$. This is a moderate increase compared to the mean-field DGP whose ELBO has complexity $\mathcal{O}(NM^2\tau L)$, while it is a clear improvement over the fully-coupled approach whose ELBO has complexity $\mathcal{O}(NM^2\tau^2L^2 + N\tau^3L^3 + M^3\tau^3L^3)$ (see Appx. D for derivations). An empirical runtime comparison is provided in Sec. 4.2.

After having discussed the advantages of the proposed approximation a remark on a disadvantage is in order: Natural gradients can not be used in this setting, since the transformation from our parameterisation to a fully-parameterised multivariate Gaussian is not invertible (see Ref. [20]). However, this is only a slight disadvantage since the stripes-and-arrow approximation has a drastically reduced number of variational parameters, compared to the fully-coupled approach, and we experimentally do not observe the same convergence problems when using standard optimisers (see Appx. E, Fig. S4).

3.3 Joint sampling of global and local latent variables

In contrast to our work, Refs. [6, 26] drop the Gaussian assumption over the inducing outputs f_M and allow instead for potentially multi-modal approximate posteriors. While their approaches are arguably more expressive than ours, their flexibility comes at a price: the distribution over the inducing outputs f_M is only given implicitly in form of Monte Carlo samples. Since the inducing outputs f_M act as global latent parameters, the noise attached to their sampling-based estimates affects all samples from one mini-batch. This can often lead to

triangular matrix such that $S_M = LL^\top$.

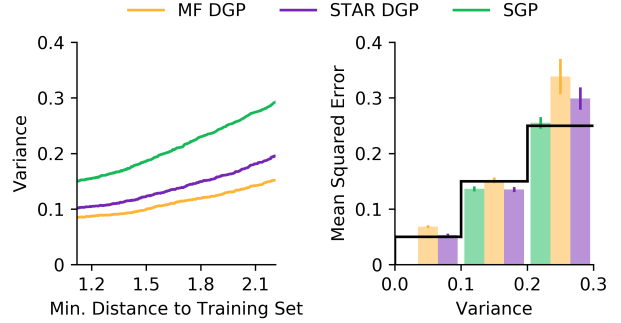


Figure 2: Calibration Study. Left: While the predicted variances increase for all methods as a function of the distance to the training data, we find that at any given distance, the uncertainty decreases from SGP to STAR DGP to MF DGP. Right: We binned the test samples according to their predicted variance and compare the empirical mean squared error of these groups with this quantity. If the mean squared error is larger than the predicted variance, the latter underestimates the uncertainty. Results are recorded on the *kin8nm* UCI dataset with a median filter for the left plot.

higher variances which may translate to slower convergence [12]. We compare to Ref. [6] in our experiments.

4 Experiments

In Sec. 4.1, we study the predictive performance of our efficient stripes-and-arrow approximation. For interpolation tasks, we found that our method performed on par with state-of-the-art approaches. However, when we additionally consider the extrapolation setting, where the test points are distant from the training points, our method outperforms its competitors due to better calibrated uncertainty estimates. In Sec. 4.2, we assess the runtime of our method and empirically confirm that our stripes-and-arrow approximation has only a negligible overhead compared to the mean-field approach and is more efficient than a fully-coupled DGP.

4.1 Benchmark Results

We compared the predictive performance of our efficient stripes-and-arrow approximation (STAR DGP) with a mean-field approximation (MF DGP) [7], stochastic gradient Hamiltonian Monte Carlo (SGHMC DGP) [6] and a sparse variational GP (SGP) [16]. As done in prior work, we reported results on a collection of eight UCI benchmark datasets and employed as evaluation criterion the average test log-likelihood.

In our initial experiments, we experienced overfitting for

Dataset (N,D)	SGP	SGHMC DGP			MF DGP		STAR DGP	
	L1	L1	L2	L3	L2	L3	L2	L3
boston (506,13)	-3.49(0.23)	-3.57(0.16)	-3.64(0.11)	-3.64(0.08)	-3.36(0.17)	-3.41(0.19)	-3.38(0.18)	-3.38(0.18)
energy (768, 8)	-2.90(0.63)	-3.22(0.69)	-3.53(0.89)	-3.26(0.75)	-3.02(0.64)	-3.45(0.86)	-3.08(0.78)	-2.95(0.74)
concrete (1030, 8)	-3.91(0.11)	-3.90(0.06)	-4.37(0.19)	-4.71(0.33)	-3.76(0.10)	-3.71(0.09)	-3.79(0.08)	-3.68(0.08)
wine red (1599,11)	-1.01(0.02)	-1.15(0.02)	-1.22(0.03)	-1.08(0.05)	-1.02(0.02)	-1.01(0.02)	-1.01(0.02)	-1.01(0.02)
kin8nm (8192, 8)	0.66(0.04)	0.72(0.03)	1.06(0.03)	0.94(0.11)	0.96(0.03)	0.98(0.04)	0.98(0.02)	0.94(0.03)
power (9568, 4)	-3.44(0.29)	-4.27(0.41)	-4.19(0.38)	-4.09(0.35)	-3.81(0.30)	-3.82(0.31)	-3.95(0.33)	-3.82(0.27)
naval (11934,16)	3.20(0.32)	2.83(0.09)	3.16(0.14)	3.18(0.12)	2.33(0.43)	2.26(0.37)	2.20(0.22)	2.95(0.27)
protein (45730, 9)	-3.20(0.04)	-3.20(0.03)	-3.17(0.02)	-3.10(0.02)	-3.31(0.04)	-3.23(0.06)	-3.23(0.04)	-3.19(0.05)

Table 1: **Extrapolation behaviour on UCI benchmark datasets.** We report test log-likelihoods (the larger, the better) for various methods and various number of layers L in the extrapolation setting. We marked all methods in bold that performed better or as good as SGP in the interpolation and extrapolation scenario, i.e., we simultaneously also looked at Tab. S2 in Appx. E. We additionally underlined those that are significantly better (non-overlapping confidence intervals) in at least one of the scenarios. Standard errors are obtained by repeating the experiment 10 times.

the variational methods. To prevent this from happening, we used 10% of the training data as a validation set. We performed early-stopping if the performance on the validation set decreased in five successive strips [27]. We did neither use a hold-out dataset for the GP methods, as they have a much smaller number of hyperparameters, nor for the Hamiltonian Monte Carlo approaches, as the correlation between adjacent samples complicates defining a good early-stopping criterion. Apart from that, we used the same model architectures, hyperparameter initialisations and optimisation settings across all methods and all datasets, which we report in Appx. E.

We assessed the interpolation behaviour of the different approaches by randomly partitioning the data into a training and a test set with a 90-10 split. To investigate the extrapolation behaviour, we created test instances that are distant from the training samples: We first randomly projected the inputs onto an one-dimensional subspace $z = Xw$, where the weights $w \in \mathbb{R}^D$ were drawn from a standard Gaussian distribution. We subsequently ordered the samples w.r.t. z and divided them accordingly into training and test set using a 50 : 50 split.

We first confirmed the reports from the literature [6, 7], that DGPs have on interpolation tasks an improved performance compared to sparse GPs (Tab. S2 in Appx. E). However, our new method was the only one that performed superior in a combined evaluation of the interpolation and the extrapolation scenarios (Tab. 1).

In the following, we further analysed these results beginning with a comparison of the variational approaches. In Fig. 2 we show that the predicted variance σ_*^2 increased as we moved away from the training data (left) while the mean squared errors also grew with larger σ_*^2 (right). The mean squared error is an empirical unbiased estimator of the variance $\text{Var}_* = \mathbb{E}[(y_* - \mu_*)^2]$ where y_* is the test

output and μ_* the mean predictor. The predicted variance σ_*^2 is also an estimator of Var_* . It is only unbiased if the method is calibrated. However, we observed for the mean-field approach that, when moving away from the training data, the mean squared error was larger than the predicted variances pointing towards underestimated uncertainties. While the mean squared error for SGP matched well with the predictive variances, the predictions are rather inaccurate as demonstrated by the large predicted variances. Our method reaches a good balance between these two methods, having generally more accurate mean predictions than the SGP and at the same time more accurate variance predictions than the MF DGP.

Next, we investigated the behaviour of the SGHMC approaches. We first ran a one-layer model that is equivalent to a sparse GP but with a different inference scheme: Instead of marginalising out the inducing outputs, they are sampled. We observed that the distribution over the inducing outputs is non-Gaussian (see Appx. E, Fig. S5), even though the optimal approximate posterior distribution is provably Gaussian in this case [11]. A possible explanation for this are convergence problems since the global latent variables are not marginalised out, which, in turn, offers a potential explanation for the poor extrapolation behaviour that we observed in our experiments across different architectures with varying number of hyperparameters and different datasets of varying size.

4.2 Runtime

We compared the impact of the variational family on the runtime as a function of the number of inducing points M , the number of layers L and the number of latent GPs τ per intermediate layer. As default architecture, we employed the same architecture as in our previous experiments ($L = 3$, $\tau = 5$, $M = 128$) and varied the pa-

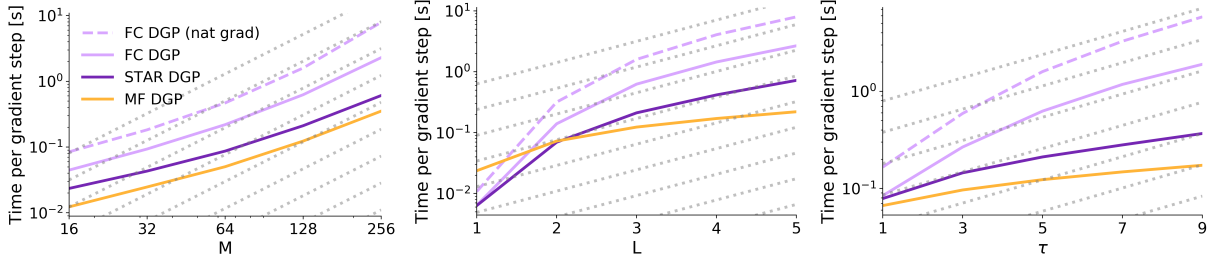


Figure 3: **Runtime comparison.** We compare the runtime of our efficient stripes-and-arrow approximation (STAR DGP) versus the fully coupled (FC DGP) and the mean-field approach (MF DGP) on the *protein* UCI dataset. Shown is the runtime of one gradient step in seconds on a logarithmic scale as a function of the number of inducing points M , the number of layers L and the number τ of latent GPs per intermediate layer (from left to right). The dotted grey lines show the theoretical scaling of the runtime of the STAR DGP for the most important term $\mathcal{O}(NM^2\tau L^2)$.

rameters independently from each other. The runtime of the different approximations was assessed for a single gradient update (for which we take $R = 5$ samples, see Alg. 2) averaged over 2000 updates on a 6 core i7-8700 CPU using a mini-batch size of 512 and the Adam optimiser [28]. For the fully-coupled (FC) variational model, we also recorded the runtime when employing natural gradients [20].

The results can be seen in Fig. 3, where, except for $L = 1$,⁵ the order from fastest to slowest method was proportional to the complexity of the variational family: mean-field, stripes-and-arrow, fully-coupled DGP. For our standard setting, $L = 3$, $\tau = 5$, $M = 128$, our STAR approximation was only two times slower than the mean-field but three times faster than FC DGP (trained with Adam). This ratio stayed almost constant when the number of inducing outputs M was changed, since the most important term in the computational costs scales as $\mathcal{O}(M^2)$ for all methods. When varying the number of layers L , we confirmed that the coupled approaches scale with $\mathcal{O}(L^2)$, while the mean-field method scales with $\mathcal{O}(L)$. When increasing the number of GPs per layer τ , we observed that in line with our theoretical findings mean-field and our sparse approximation scale more favourably than the fully-coupled DGP.

5 Summary

In this paper, we investigated a new class of variational families for deep GPs. Our approach is (i) efficient as it allows to marginalise over the global latent variables and (ii) expressive as it couples the inducing outputs across layers in the variational posterior. Naively coupling all inducing outputs does not scale to large datasets, hence

⁵In comparison to the implementation of Ref. [7], we use a different (faster) scheme to obtain R samples in the first layer, which leads to the observed difference.

we suggest a sparse and structured approximation that only takes the most important dependencies into account. It is competitive with the mean-field approach [7] on standard interpolation tasks and outperforms its competitors if the test points are distant from the training points.

Our stripes-and-arrow approximation is only one way of coupling the latent GPs. Discovering new variational families that either allow for more speed-ups by applying Kronecker factorisations as done in the context of neural networks [29] or for optimisation using natural gradients [20] is an interesting direction of future work.

There has been a lot of follow-up work on deep GPs in which the probabilistic model is altered to allow for multiple outputs [30], multiple input sources [31], latent features [21] or for interpreting the latent states as differential flows [32]. Our approach can be easily adapted to any of these models and is therefore a useful addition to the current set of inference engines for deep GP models.

References

- [1] C. Rasmussen and C. Williams, *Gaussian Processes for Machine Learning*. The MIT Press, 2005.
- [2] D. Reeb, A. Doerr, S. Gerwinn, and B. Rakitsch, “Learning gaussian processes by minimizing pac-bayesian generalization bounds,” in *Advances in Neural Information Processing Systems*, 2018.
- [3] A. Hebbal, L. Brevault, M. Balesdent, E.-G. Talbi, and N. Melab, “Bayesian optimization using deep gaussian processes,” *arXiv preprint arXiv:1905.03350*, 2019.
- [4] C. Zimmer, M. Meister, and D. Nguyen-Tuong, “Safe active learning for time-series modeling with

- gaussian processes,” in *Advances in Neural Information Processing Systems*, 2018.
- [5] A. Damianou and N. Lawrence, “Deep gaussian processes,” in *Artificial Intelligence and Statistics*, 2013.
- [6] M. Havasi, J. Lobato, and J. Fuentes, “Inference in deep gaussian processes using stochastic gradient hamiltonian monte carlo,” in *Advances in Neural Information Processing Systems*, 2018.
- [7] H. Salimbeni and M. Deisenroth, “Doubly stochastic variational inference for deep gaussian processes,” in *Advances in Neural Information Processing Systems*, 2017.
- [8] T. Bui, D. Hernández-Lobato, J. Hernandez-Lobato, Y. Li, and R. Turner, “Deep gaussian processes for regression using approximate expectation propagation,” in *International Conference on Machine Learning*, 2016.
- [9] D. Blei, A. Kucukelbir, and J. McAuliffe, “Variational inference: A review for statisticians,” *Journal of the American Statistical Association*, 2017.
- [10] E. Snelson and Z. Ghahramani, “Sparse gaussian processes using pseudo-inputs,” in *Advances in Neural Information Processing Systems*, 2006.
- [11] M. Titsias, “Variational learning of inducing variables in sparse gaussian processes,” in *Artificial Intelligence and Statistics*, 2009.
- [12] D. Kingma, T. Salimans, and M. Welling, “Variational dropout and the local reparameterization trick,” in *Advances in Neural Information Processing Systems*, 2015.
- [13] R. Turner and M. Sahani, “Two problems with variational expectation maximisation for time-series models,” *Bayesian Time Series Models*, 2011.
- [14] D. Amodei, C. Olah, J. Steinhardt, P. Christiano, J. Schulman, and D. Mané, “Concrete problems in ai safety,” *arXiv preprint arXiv:1606.06565*, 2016.
- [15] J. Snoek, Y. Ovia, E. Fertig, B. Lakshminarayanan, S. Nowozin, D. Sculley, J. Dillon, J. Ren, and Z. Nado, “Can you trust your model’s uncertainty? evaluating predictive uncertainty under dataset shift,” in *Advances in Neural Information Processing Systems*, 2019.
- [16] J. Hensman, N. Fusi, and N. Lawrence, “Gaussian processes for big data,” *Conference on Uncertainty in Artificial Intelligence*, 2013.
- [17] D. Duvenaud, O. Rippel, R. P. Adams, and Z. Ghahramani, “Avoiding pathologies in very deep networks,” in *Artificial Intelligence and Statistics*, 2014.
- [18] D. Rezende, S. Mohamed, and D. Wierstra, “Stochastic backpropagation and approximate inference in deep generative models,” in *International Conference on Machine Learning*, 2014.
- [19] S.-I. Amari, “Natural gradient works efficiently in learning,” *Neural Computation*, 1998.
- [20] H. Salimbeni, S. Eleftheriadis, and J. Hensman, “Natural gradients in practice: Non-conjugate variational inference in gaussian process models,” in *Artificial Intelligence and Statistics*, 2018.
- [21] H. Salimbeni, V. Dutoit, J. Hensman, and M. P. Deisenroth, “Deep gaussian processes with importance-weighted variational inference,” *International Conference on Machine Learning*, 2019.
- [22] I. Ustyuzhaninov, I. Kazlauskaitė, M. Kaiser, E. Bodin, N. D. F. Campbell, and C. H. Ek, “Compositional uncertainty in deep gaussian processes,” *arXiv preprint arXiv:1909.07698v3 (25 Feb 2020)*, 2020.
- [23] A. Matthews, M. Van Der Wilk, T. Nickson, K. Fujii, A. Boukouvalas, P. León-Villagrà, Z. Ghahramani, and J. Hensman, “Gpflow: A gaussian process library using tensorflow,” *Journal of Machine Learning Research*, 2017.
- [24] M. Abadi, P. Barham, J. Chen, Z. Chen, A. Davis, J. Dean, M. Devin, S. Ghemawat, G. Irving, M. Isard, *et al.*, “Tensorflow: a system for large-scale machine learning,” in *USENIX Symposium on Operating Systems Design and Implementation*, 2016.
- [25] D. Smolarski, “Diagonally-stripped matrices and approximate inverse preconditioners,” *Journal of Computational and Applied Mathematics*, 2006.
- [26] H. Yu, Y. Chen, Z. Dai, K. H. Low, and P. Jaillet, “Implicit posterior variational inference for deep gaussian processes,” in *Advances in Neural Information Processing Systems*, 2019.
- [27] L. Prechelt, “Early stopping-but when?,” in *Neural Networks: Tricks of the trade*, Springer, 1998.
- [28] D. Kingma and J. Ba, “Adam: A method for stochastic optimization,” in *International Conference of Learning Representations*, 2015.

- [29] J. Martens and R. Grosse, “Optimizing neural networks with kronecker-factored approximate curvature,” in *International Conference on Machine Learning*, 2015.
- [30] M. Kaiser, C. Otte, T. Runkler, and C. H. Ek, “Bayesian alignments of warped multi-output gaussian processes,” in *Advances in Neural Information Processing Systems*, 2018.
- [31] O. Hamelijnck, T. Damoulas, K. Wang, and M. Girolami, “Multi-resolution multi-task gaussian processes,” in *Advances in Neural Information Processing Systems*, 2019.
- [32] P. Hegde, M. Heinonen, H. Lähdesmäki, and S. Kaski, “Deep learning with differential gaussian process flows,” in *Artificial Intelligence and Statistics*, 2019.

Supplementary material for

Beyond the Mean-Field: Structured Deep Gaussian Processes Improve the Predictive Uncertainties

A Marginalisation of the inducing outputs (proof of Theorem 1)

The aim of this section is to provide a complete proof for Thm. 1. We will do this by starting from the formula for $q(f_n^l)$ that we work out in Appx. C,

$$q(f_n^L) = \int \left[\int q(f_M) \prod_{l=1}^L p(f_n^l | f_M^l; f_n^{l-1}) df_M \right] df_n^1 \cdots df_n^{L-1}. \quad (27)$$

Comparing to Eq. (17), we see that it remains to be shown that indeed

$$\int q(f_M) \prod_{l=1}^L p(f_n^l | f_M^l; f_n^{l-1}) df_M = \prod_{l=1}^L q(f_n^l | f_n^1, \dots, f_n^{l-1}), \quad (28)$$

where the distributions q on the right hand side have the properties described in Eqs. (18) - (22). The terms appearing on the left hand side are given by $q(f_M) = \mathcal{N}(f_M | \mu_M, S_M)$, which is interchangeably also denoted as

$$q(f_M^{1:L}) = \mathcal{N}(f_M^{1:L} | \mu_M^{1:L}, S_M^{1:L}) = q \left(\begin{pmatrix} f_M^1 \\ \vdots \\ f_M^L \end{pmatrix} \right) = \mathcal{N} \left(\left(\begin{pmatrix} f_M^1 \\ \vdots \\ f_M^L \end{pmatrix} \right) \middle| \begin{pmatrix} \mu_M^1 \\ \vdots \\ \mu_M^L \end{pmatrix}, \begin{pmatrix} S_M^{11} & \cdots & S_M^{1L} \\ \vdots & \ddots & \vdots \\ S_M^{L1} & \cdots & S_M^{LL} \end{pmatrix} \right), \quad (29)$$

and

$$p(f_n^l | f_M^l; f_n^{l-1}) = \mathcal{N}(f_n^l | \tilde{\mathcal{K}}_{nM}^l f_M^l, \tilde{\mathcal{K}}_{nn}^l), \quad (30)$$

where

$$\tilde{\mathcal{K}}_{nM}^l = \mathcal{K}_{nM}^l (\mathcal{K}_{MM}^l)^{-1} \quad (31)$$

$$\tilde{\mathcal{K}}_{nn}^l = \mathcal{K}_{nn}^l - \mathcal{K}_{nM}^l (\mathcal{K}_{MM}^l)^{-1} \mathcal{K}_{Mn}^l. \quad (32)$$

In order to show that Eq. (28) holds, we will introduce a rather technical lemma in the following and prove it later by induction.

Lemma 2. *Given the definitions in Eqs. (29) and (30), $\forall l = 1, \dots, L$ we have*

$$\int q(f_M^{1:L}) \prod_{l'=1}^L p(f_n^{l'} | f_M^{l'}) df_M^{l'} = \left[\prod_{l'=1}^{l-1} q(f_n^{l'} | f_n^{1:l'-1}) \right] \int q(f_n^l, f_M^{l+1:L} | f_n^{1:l-1}) \prod_{l'=l+1}^L p(f_n^{l'} | f_M^{l'}) df_M^{l'}, \quad (33)$$

where $q(f_n^{l'} | f_n^{1:l'-1})$ is as in Eq. (18) and

$$q(f_n^l, f_M^{l+1:L} | f_n^{1:l-1}) = \mathcal{N} \left(\begin{pmatrix} f_n^l \\ f_M^{l+1:L} \end{pmatrix} \middle| \begin{pmatrix} \hat{\mu}_n^l \\ \hat{\mu}_M^{l+1:L} \end{pmatrix}, \begin{pmatrix} \hat{\Sigma}_n^l & \\ & {}^l \hat{\Sigma}_{nM}^{l,l+1:L} \end{pmatrix} \right). \quad (34)$$

Here $\hat{\mu}_n^l$ and $\hat{\Sigma}_n^l$ are as in Eqs. (19) and (20), respectively, and we defined

$$\begin{aligned} {}^l \hat{\mu}_M^{l+1:L} &= \mu_M^{l+1:L} + S_M^{l+1:L,1:l-1} \text{diag}(\tilde{\mathcal{K}}_{Mn}^{1:l-1}) \left(\tilde{S}_n^{1:l-1,1:l-1} \right)^{-1} (f_n^{1:l-1} - \tilde{\mu}_n^{1:l-1}) \\ {}^l \hat{\Sigma}_M^{l+1:L,l+1:L} &= S_M^{l+1:L,l+1:L} - S_M^{l+1:L,1:l-1} \text{diag}(\tilde{\mathcal{K}}_{Mn}^{1:l-1}) \left(\tilde{S}_n^{1:l-1,1:l-1} \right)^{-1} \text{diag}(\tilde{\mathcal{K}}_{nM}^{1:l-1}) S_M^{1:l-1,l+1:L} \\ {}^l \hat{\Sigma}_{nM}^{l,l+1:L} &= \tilde{\mathcal{K}}_{nM}^l S_M^{l,l+1:L} - \tilde{S}_n^{1:l-1,1:l-1} \left(\tilde{S}_n^{1:l-1,1:l-1} \right)^{-1} \text{diag}(\tilde{\mathcal{K}}_{nM}^{1:l-1}) S_M^{1:l-1,l+1:L}. \end{aligned} \quad (35)$$

In the equations above we used $\text{diag}(A^{1:l})$ to denote the formation of a block diagonal matrix, where the diagonal blocks are given by A^1, \dots, A^l . Note that while we only need one index to label $\hat{\mu}_n^l$ and $\hat{\Sigma}_n^l$, we need several for the objects defined in Eq. (35). Take e.g. ${}^{l\hat{\Sigma}_M^{l+1:L, l+1:L}}$: The upper left index denotes for which l the formula is valid (which will become important when we do the induction step $l \rightarrow l+1$). The upper right indices (try to) capture which terms of S_M are most important for the definition, they have nothing to do with the dimensionality of the objects. (In fact, the matrix ${}^{l\hat{\Sigma}_M}$ contains $L-l-1 \times L-l-1$ blocks of various sizes $T_l M \times T_{l'} M$.) This makes it easier later on when we do calculations with these objects.

Before we prove Lem. 2, we will first show how its results can be used to prove Thm. 1:

Proof of Theorem 1. As shown in Appx. C, we can write

$$q(f_n^L) = \int \left[\int q(f_M) \prod_{l=1}^L p(f_n^l | f_M^l; f_n^{l-1}) df_M \right] df_n^1 \dots df_n^{L-1}. \quad (36)$$

Obtaining a formula for the inner integral can be done using Lem. 2 with $l = L$, in which case Eq. (33) reads

$$\int q(f_M^1, \dots, f_M^L) \prod_{l'=1}^L p(f_n^{l'} | f_M^{l'}) df_M^{l'} = \left[\prod_{l'=1}^{L-1} q(f_n^{l'} | f_n^1, \dots, f_n^{l'-1}) \right] q(f_n^L | f_n^1, \dots, f_n^{L-1}) \quad (37)$$

since there is nothing left to integrate over. According to Eqs. (18) and (34) the distribution $q(f_n^L | f_n^1, \dots, f_n^{L-1})$ has the form necessary to be written as part of the product and we therefore have

$$\int q(f_M^1, \dots, f_M^L) \prod_{l'=1}^L p(f_n^{l'} | f_M^{l'}) df_M^{l'} = \prod_{l'=1}^L q(f_n^{l'} | f_n^1, \dots, f_n^{l'-1}). \quad (38)$$

Plugging this into Eq. (36) yields

$$q(f_n^L) = \int \prod_{l'=1}^L q(f_n^{l'} | f_n^1, \dots, f_n^{l'-1}) df_n^1 \dots df_n^{L-1}, \quad (39)$$

where the distributions q on the right hand side have the properties described in Eqs. (18) - (22). \square

In order to prove Lem. 2, we will regularly need two standard formulas from Gaussian calculus, namely conditioning multivariate Gaussians,

$$\mathcal{N} \left(\begin{pmatrix} x \\ y \end{pmatrix} \middle| \begin{pmatrix} a \\ b \end{pmatrix}, \begin{pmatrix} A & C \\ C^\top & B \end{pmatrix} \right) = \mathcal{N}(x|a, A) \mathcal{N}(y|b + C^\top A^{-1}(x-a), B - C^\top A^{-1}C), \quad (40)$$

and solving Gaussian integrals ("propagation"):

$$\int \mathcal{N}(x|a + Fy, A) \mathcal{N}(y|b, B) dy = \mathcal{N}(x|a + Fb, A + FBF^\top). \quad (41)$$

Proof of Lemma 2. As already said, we prove the lemma by induction:

Base case We need to show that Eq. (33) holds for $l = 1$, i.e., that

$$\int q(f_M^1, \dots, f_M^L) \prod_{l'=1}^L p(f_n^{l'} | f_M^{l'}) df_M^{l'} = \int q(f_n^1, f_M^2, \dots, f_M^L) \prod_{l'=2}^L p(f_n^{l'} | f_M^{l'}) df_M^{l'}, \quad (42)$$

where $q(f_n^1, f_M^2, \dots, f_M^L)$ is given according to Eqs. (34) and (35).

In order to do so, we will perform the following steps:

i) Starting with the LHS of Eq. (42), we isolate all terms that depend on f_M^1 :

$$\int \left[\int q(f_M^1, \dots, f_M^L) p(f_n^1 | f_M^1) df_M^1 \right] \prod_{l'=2}^L p(f_n^{l'} | f_M^{l'}) df_M^{l'}. \quad (43)$$

ii) In the previous equation, we only consider the inner integral and condition q on f_M^1 :

$$\int q(f_M^1, \dots, f_M^L) p(f_n^1 | f_M^1) df_M^1 = \int q(f_M^1) q(f_M^2, \dots, f_M^L | f_M^1) p(f_n^1 | f_M^1) df_M^1. \quad (44)$$

iii) Next, we obtain the joint distribution of the two terms that are conditioned on f_M^1 :

$$\int q(f_M^1) q(f_M^2, \dots, f_M^L | f_M^1) p(f_n^1 | f_M^1) df_M^1 = \int q(f_M^1) q(f_n^1, f_M^2, \dots, f_M^L | f_M^1) df_M^1. \quad (45)$$

iv) Then we evaluate the integral:

$$\int q(f_M^1) q(f_n^1, f_M^2, \dots, f_M^L | f_M^1) df_M^1 = q(f_n^1, f_M^2, \dots, f_M^L). \quad (46)$$

v) Finally, we check that the resulting distribution is given by Eqs. (34) and (35). This then proves the equality in Eq. (42).

Step ii) is the first one where we actually need to calculate something, namely the conditioning of $q(f_M^1, \dots, f_M^L)$. Using its definition in Eq. (29) and performing the conditioning according to Eq. (40) yields

$$\begin{aligned} q(f_M^1, \dots, f_M^L) &= q(f_M^1) q(f_M^2, \dots, f_M^L | f_M^1) \\ &= \mathcal{N}(f_M^1 | \mu_M^1, S_M^{11}) \mathcal{N}\left(f_M^{2:L} \middle| \mu_M^{2:L} + S_M^{2:L,1} (S_M^{11})^{-1} (f_M^1 - \mu_M^1), S_M^{2:L,2:L} - S_M^{2:L,1} (S_M^{11})^{-1} S_M^{1,2:L}\right). \end{aligned} \quad (47)$$

For step iii) we use the formula we just obtained for $q(f_M^2, \dots, f_M^L | f_M^1)$ and additionally $p(f_n^1 | f_M^1)$, which, according to Eq. (30) is given by $\mathcal{N}\left(f_n^1 \middle| \tilde{\mathcal{K}}_{nM}^1 f_M^1, \tilde{\mathcal{K}}_{nn}^1\right)$, and then proceed to build their joint Gaussian distribution:

$$\begin{aligned} q(f_n^1, f_M^2, \dots, f_M^L | f_M^1) &= p(f_n^1 | f_M^1) q(f_M^2, \dots, f_M^L | f_M^1) \\ &= \mathcal{N}\left(\begin{pmatrix} f_n^1 \\ f_M^{2:L} \end{pmatrix} \middle| \begin{pmatrix} \tilde{\mathcal{K}}_{nM}^1 f_M^1 \\ \mu_M^{2:L} + S_M^{2:L,1} (S_M^{11})^{-1} (f_M^1 - \mu_M^1) \end{pmatrix}, \begin{pmatrix} \tilde{\mathcal{K}}_{nn}^1 & 0 \\ 0 & S_M^{2:L,2:L} - S_M^{2:L,1} (S_M^{11})^{-1} S_M^{1,2:L} \end{pmatrix}\right). \end{aligned} \quad (48)$$

In step iv) we perform the integration using the term above for the joint and $q(f_M^1) = \mathcal{N}(f_M^1 | \mu_M^1, S_M^{11})$ from Eq. (47) for the marginal. Applying Eq. (41) yields

$$\begin{aligned} &\int q(f_n^1, f_M^2, \dots, f_M^L | f_M^1) q(f_M^1) df_M^1 \\ &= \mathcal{N}\left(\begin{pmatrix} f_n^1 \\ f_M^{2:L} \end{pmatrix} \middle| \begin{pmatrix} \tilde{\mathcal{K}}_{nM}^1 \mu_M^1 \\ \mu_M^{2:L} + S_M^{2:L,1} (S_M^{11})^{-1} (\mu_M^1 - \mu_M^1) \end{pmatrix}, \begin{pmatrix} \tilde{\mathcal{K}}_{nn}^1 & 0 \\ 0 & S_M^{2:L,2:L} - S_M^{2:L,1} (S_M^{11})^{-1} S_M^{1,2:L} \end{pmatrix} + \begin{pmatrix} \tilde{\mathcal{K}}_{nM}^1 \\ S_M^{2:L,1} (S_M^{11})^{-1} \end{pmatrix} S_M^{11} \begin{pmatrix} \tilde{\mathcal{K}}_{nM}^1 \\ S_M^{2:L,1} (S_M^{11})^{-1} \end{pmatrix}^\top\right) \\ &= \mathcal{N}\left(\begin{pmatrix} f_n^1 \\ f_M^{2:L} \end{pmatrix} \middle| \begin{pmatrix} \tilde{\mu}_n^1 \\ \mu_M^{2:L} \end{pmatrix}, \begin{pmatrix} \tilde{S}_n^{11} & \tilde{\mathcal{K}}_{nM}^1 S_M^{1,2:L} \\ S_M^{2:L,1} \tilde{\mathcal{K}}_{Mn}^1 & S_M^{2:L,2:L} \end{pmatrix}\right). \end{aligned} \quad (49)$$

In order to arrive at the last line we simplified the terms and used the definitions in Eqs. (21) and (22).

Step v) requires us to evaluate Eq. (34) for $l = 1$ resulting in

$$\mathcal{N} \left(\begin{pmatrix} f_n^1 \\ f_M^{2:L} \end{pmatrix} \middle| \begin{pmatrix} \hat{\mu}_n^1 \\ 1 \hat{\mu}_M^{2:L} \end{pmatrix}, \begin{pmatrix} \hat{\Sigma}_n^1 & 1 \hat{\Sigma}_{nM}^{1,2:L} \\ (1 \hat{\Sigma}_{nM}^{l,2:L})^\top & 1 \hat{\Sigma}_M^{2:L,2:L} \end{pmatrix} \right), \quad (50)$$

which is the term $q(f_n^1, f_M^2, \dots, f_M^L)$ on the RHS of Eq. (42). Plugging in the definitions from Eq. (35) we can easily verify that this last term indeed agrees with Eq. (49). Therefore our statement in Lem. 2 holds for $l = 1$.

Inductive step We assume that Lemma 2 holds for some $l = 1, \dots, L - 1$ (induction hypothesis) and then need to show that it also holds for $l + 1$. That is, assuming that

$$\int q(f_M^{1:L}) \prod_{l'=1}^L p(f_n^{l'} | f_M^{l'}) df_M^{l'} = \left[\prod_{l'=1}^{l-1} q(f_n^{l'} | f_n^{1:l'-1}) \right] \int q(f_n^l, f_M^{l+1:L} | f_n^{1:l-1}) \prod_{l'=l+1}^L p(f_n^{l'} | f_M^{l'}) df_M^{l'}, \quad (51)$$

holds for some l with the terms on the RHS given by Eqs. (34), and (35) we need to show that we can also write the previous equation as

$$\left[\prod_{l'=1}^l q(f_n^{l'} | f_n^{1:l'-1}) \right] \int q(f_n^{l+1}, f_M^{l+2:L} | f_n^{1:l}) \prod_{l'=l+2}^L p(f_n^{l'} | f_M^{l'}) df_M^{l'}, \quad (52)$$

where this time the terms are given by Eqs. (34), and (35) but with $l \rightarrow l + 1$.

The way to show this is very similar to the way we showed the base case, the resulting formulas will only look more complicated and we will need one additional step in the beginning:

- o) Assuming that Eq. (51) holds for some l , we can start immediately with the RHS. The first step will be to marginalise f_n^l from the distribution q within the integral and show that the resulting marginal $q(f_n^l | f_n^{1:l-1})$ has the right form to be written as part of the product in front of the integral:

$$\left[\prod_{l'=1}^{l-1} q(f_n^{l'} | f_n^{1:l'-1}) \right] \int q(f_n^l, f_M^{l+1:L} | f_n^{1:l-1}) \prod_{l'=l+1}^L p(f_n^{l'} | f_M^{l'}) df_M^{l'} \quad (53)$$

$$= \left[\prod_{l'=1}^{l-1} q(f_n^{l'} | f_n^{1:l'-1}) \right] \int q(f_n^l | f_n^{1:l-1}) q(f_M^{l+1:L} | f_n^{1:l}) \prod_{l'=l+1}^L p(f_n^{l'} | f_M^{l'}) df_M^{l'} \quad (54)$$

$$= \left[\prod_{l'=1}^l q(f_n^{l'} | f_n^{1:l'-1}) \right] \int q(f_M^{l+1:L} | f_n^{1:l}) \prod_{l'=l+1}^L p(f_n^{l'} | f_M^{l'}) df_M^{l'}. \quad (55)$$

Having done this, we will have to do the exact same steps as in the base case, which we will repeat below with updated indices.

- i) Continuing from Eq. (55), we isolate all terms that depend on f_M^{l+1} :

$$\left[\prod_{l'=1}^l q(f_n^{l'} | f_n^{1:l'-1}) \right] \int \left[\int q(f_M^{l+1:L} | f_n^{1:l}) p(f_n^{l+1} | f_M^{l+1}) df_M^{l+1} \right] \prod_{l'=l+2}^L p(f_n^{l'} | f_M^{l'}) df_M^{l'}. \quad (56)$$

- ii) Comparing this to Eq. (52), we see that it remains to be shown that the inner integral equals $q(f_n^{l+1}, f_M^{l+2:L} | f_n^{1:l})$ [given by Eqs. (34) and (35)]. Therefore we only consider the inner integral and therein condition q on f_M^{l+1} :

$$\int q(f_M^{l+1:L} | f_n^{1:l}) p(f_n^{l+1} | f_M^{l+1}) df_M^{l+1} = \int q(f_M^{l+1} | f_n^{1:l}) q(f_M^{l+2:L} | f_n^{1:l}, f_M^{l+1}) p(f_n^{l+1} | f_M^{l+1}) df_M^{l+1}. \quad (57)$$

iii) Next, we obtain the joint distribution of the two terms that are conditioned on f_M^{l+1} :

$$\int q(f_M^{l+1}|f_n^{1:l})q(f_M^{l+2:L}|f_n^{1:l}, f_M^{l+1})p(f_n^{l+1}|f_M^{l+1})df_M^{l+1} = \int q(f_M^{l+1}|f_n^{1:l})q(f_n^{l+1}, f_M^{l+2:L}|f_n^{1:l}, f_M^{l+1})df_M^{l+1}. \quad (58)$$

iv) Then we evaluate the integral:

$$\int q(f_M^{l+1}|f_n^{1:l})q(f_n^{l+1}, f_M^{l+2:L}|f_n^{1:l}, f_M^{l+1})df_M^{l+1} = q(f_n^{l+1}, f_M^{l+2:L}|f_n^{1:l}). \quad (59)$$

v) Finally, we check that the resulting distribution is given by Eqs. (34) and (35). This then proves the equality of Eqs. (51) and (52).

Let us begin with step o): According to Eq. (34), we have

$$q(f_n^l, f_M^{l+1:L}|f_n^{1:l-1}) = \mathcal{N}\left(\begin{pmatrix} f_n^l \\ f_M^{l+1:L} \end{pmatrix} \middle| \begin{pmatrix} \hat{\mu}_n^l \\ \hat{\mu}_M^{l+1:L} \end{pmatrix}, \begin{pmatrix} \hat{\Sigma}_n^l & {}^l\hat{\Sigma}_{nM}^{l,l+1:L} \\ ({}^l\hat{\Sigma}_{nM}^{l,l+1:L})^\top & {}^l\hat{\Sigma}_M^{l+1:L,l+1:L} \end{pmatrix}\right), \quad (60)$$

which we condition on f_n^l using Eq. (40) (i.e., going from Eq. (53) to Eq. (54)):

$$\begin{aligned} q(f_n^l, f_M^{l+1:L}|f_n^{1:l-1}) &= q(f_n^l|f_n^{1:l-1})q(f_M^{l+1:L}|f_n^{1:l}) = \mathcal{N}\left(f_n^l \middle| \hat{\mu}_n^l, \hat{\Sigma}_n^l\right) \times \\ &\mathcal{N}\left(f_M^{l+1:L} \middle| {}^l\hat{\mu}_M^{l+1:L} + ({}^l\hat{\Sigma}_{nM}^{l+1:L,l})^\top (\hat{\Sigma}_n^l)^{-1} (f_n^l - \hat{\mu}_n^l), {}^l\hat{\Sigma}_M^{l+1:L,l+1:L} - ({}^l\hat{\Sigma}_{nM}^{l+1:L,l})^\top (\hat{\Sigma}_n^l)^{-1} {}^l\hat{\Sigma}_{nM}^{l,l+1:L}\right). \end{aligned} \quad (61)$$

We therefore see that $q(f_n^l|f_n^{1:l-1}) = \mathcal{N}\left(f_n^l \middle| \hat{\mu}_n^l, \hat{\Sigma}_n^l\right)$, which is the right form for it to be included in the product in front of the integral in Eq. (54). This lets us arrive at Eq. (55), hence finishing step o).

In step i) nothing really happens, we just note that, according to Eq. (30),

$$p(f_n^{l+1}|f_M^{l+1}) = \mathcal{N}\left(f_n^{l+1} \middle| \tilde{\mathcal{K}}_{nM}^{l+1} f_M^{l+1}, \tilde{\mathcal{K}}_{nn}^{l+1}\right). \quad (62)$$

Using $q(f_M^{l+1:L}|f_n^{1:l})$ from Eq. (61), we perform step ii) according to Eq. (40), resulting in

$$q(f_M^{l+1:L}|f_n^{1:l}) = q(f_M^{l+1}|f_n^{1:l})q(f_M^{l+2:L}|f_n^{1:l}, f_M^{l+1}), \quad (63)$$

where

$$q(f_M^{l+1}|f_n^{1:l}) = \mathcal{N}\left(f_M^{l+1} \middle| {}^l\hat{\mu}_M^{l+1} + ({}^l\hat{\Sigma}_{nM}^{l+1,l})^\top (\hat{\Sigma}_n^l)^{-1} (f_n^l - \hat{\mu}_n^l), {}^l\hat{\Sigma}_M^{l+1,l+1} - ({}^l\hat{\Sigma}_{nM}^{l+1,l})^\top (\hat{\Sigma}_n^l)^{-1} {}^l\hat{\Sigma}_{nM}^{l,l+1}\right) \quad (64)$$

and

$$\begin{aligned} &q(f_M^{l+2:L}|f_n^{1:l}, f_M^{l+1}) \\ &= \mathcal{N}\left(f_M^{l+2:L} \middle| {}^l\hat{\mu}_M^{l+2:L} + ({}^l\hat{\Sigma}_{nM}^{l+2:L,l})^\top (\hat{\Sigma}_n^l)^{-1} (f_n^l - \hat{\mu}_n^l) + ({}^l\hat{\Sigma}_M^{l+2:L,l+1} - ({}^l\hat{\Sigma}_{nM}^{l+2:L,l})^\top (\hat{\Sigma}_n^l)^{-1} {}^l\hat{\Sigma}_{nM}^{l,l+1}) \times \right. \\ &\quad \left. ({}^l\hat{\Sigma}_M^{l+1,l+1} - ({}^l\hat{\Sigma}_{nM}^{l+1,l})^\top (\hat{\Sigma}_n^l)^{-1} {}^l\hat{\Sigma}_{nM}^{l,l+1})^{-1} (f_M^{l+1} - {}^l\hat{\mu}_M^{l+1} - ({}^l\hat{\Sigma}_{nM}^{l+1,l})^\top (\hat{\Sigma}_n^l)^{-1} (f_n^l - \hat{\mu}_n^l)), \right. \\ &\quad \left. {}^l\hat{\Sigma}_M^{l+2:L,l+2:L} - ({}^l\hat{\Sigma}_{nM}^{l+2:L,l})^\top (\hat{\Sigma}_n^l)^{-1} {}^l\hat{\Sigma}_{nM}^{l,l+2:L} - ({}^l\hat{\Sigma}_M^{l+2:L,l+1} - ({}^l\hat{\Sigma}_{nM}^{l+2:L,l})^\top (\hat{\Sigma}_n^l)^{-1} {}^l\hat{\Sigma}_{nM}^{l,l+1}) \times \right. \\ &\quad \left. ({}^l\hat{\Sigma}_M^{l+1,l+1} - ({}^l\hat{\Sigma}_{nM}^{l+1,l})^\top (\hat{\Sigma}_n^l)^{-1} {}^l\hat{\Sigma}_{nM}^{l,l+1})^{-1} ({}^l\hat{\Sigma}_M^{l+1,l+2:L} - ({}^l\hat{\Sigma}_{nM}^{l+1,l})^\top (\hat{\Sigma}_n^l)^{-1} {}^l\hat{\Sigma}_{nM}^{l,l+2:L})\right). \end{aligned} \quad (65)$$

For step iii) we have to build the joint Gaussian distribution

$$q(f_M^{l+2:L} | f_n^{1:l}, f_M^{l+1}) p(f_n^{l+1} | f_M^{l+1}) = q(f_n^{l+1}, f_M^{l+2:L} | f_n^{1:l}, f_M^{l+1}) \quad (66)$$

using Eqs. (62) and (65). Since this formula would be even longer than the one in Eq. (65), we refrain from explicitly writing it here. While the corresponding formula for the base case [Eq. (48)] is much simpler the resulting form of Eq. (66) would be similar.

Next, the integration in step iv) can be performed using Eqs. (41), (64), and (66). The calculations are again very similar to the ones in the corresponding step for the base case [Eq. (49)] so we only state the final result here:

$$\begin{aligned} q(f_n^{l+1}, f_M^{l+2:L} | f_n^{1:l}) &= \int q(f_M^{l+1} | f_n^{1:l}) q(f_n^{l+1}, f_M^{l+2:L} | f_n^{1:l}, f_M^{l+1}) d f_M^{l+1} \\ &= \mathcal{N} \left(\begin{pmatrix} f_n^{l+1} \\ f_M^{l+2:L} \end{pmatrix} \middle| \begin{pmatrix} \hat{m}_n^{l+1} \\ \hat{m}_M^{l+2:L} \end{pmatrix}, \begin{pmatrix} \hat{S}_n^{l+1} & \hat{S}_{nM}^{l+1, l+2:L} \\ (\hat{S}_{nM}^{l+1, l+2:L})^\top & \hat{S}_M^{l+2:L, l+2:L} \end{pmatrix} \right), \end{aligned} \quad (67)$$

where

$$\hat{m}_n^{l+1} = \tilde{\mathcal{K}}_{nM}^{l+1} \left({}^l \hat{\mu}_M^{l+1} + \left({}^l \hat{\Sigma}_{nM}^{l+1, l} \right)^\top \left(\hat{\Sigma}_n^l \right)^{-1} (f_n^l - \hat{\mu}_n^l) \right) \quad (68)$$

$$\hat{m}_M^{l+2:L} = {}^l \hat{\mu}_M^{l+2:L} + \left({}^l \hat{\Sigma}_{nM}^{l+2:L, l} \right)^\top \left(\hat{\Sigma}_n^l \right)^{-1} (f_n^l - \hat{\mu}_n^l) \quad (69)$$

$$\hat{S}_n^{l+1} = \mathcal{K}_{nn}^{l+1} + \mathcal{K}_{nM}^{l+1} \left({}^l \hat{\Sigma}_M^{l+1, l+1} - \left({}^l \hat{\Sigma}_{nM}^{l+1, l} \right)^\top \left(\hat{\Sigma}_n^l \right)^{-1} {}^l \hat{\Sigma}_{nM}^{l, l+1} \right) \mathcal{K}_{Mn}^{l+1} \quad (70)$$

$$\hat{S}_{nM}^{l+1, l+2:L} = \tilde{\mathcal{K}}_{nM}^{l+1} \left({}^l \hat{\Sigma}_M^{l+1, l+2:L} - \left({}^l \hat{\Sigma}_{nM}^{l+1, l} \right)^\top \left(\hat{\Sigma}_n^l \right)^{-1} {}^l \hat{\Sigma}_{nM}^{l, l+2:L} \right) \quad (71)$$

$$\hat{S}_M^{l+2:L, l+2:L} = {}^l \hat{\Sigma}_M^{l+2:L, l+2:L} - \left({}^l \hat{\Sigma}_{nM}^{l+2:L, l} \right)^\top \left(\hat{\Sigma}_n^l \right)^{-1} {}^l \hat{\Sigma}_{nM}^{l, l+2:L}. \quad (72)$$

What remains to be shown in step v) is that this result does infact agree with the expected result from Lem. 2, i.e.,

$$q(f_n^{l+1}, f_M^{l+2:L} | f_n^{1:l}) = \mathcal{N} \left(\begin{pmatrix} f_n^{l+1} \\ f_M^{l+2:L} \end{pmatrix} \middle| \begin{pmatrix} \hat{\mu}_n^{l+1} \\ {}^{l+1} \hat{\mu}_M^{l+2:L} \end{pmatrix}, \begin{pmatrix} \hat{\Sigma}_n^{l+1} & {}^{l+1} \hat{\Sigma}_{nM}^{l+1, l+2:L} \\ ({}^{l+1} \hat{\Sigma}_{nM}^{l+1, l+2:L})^\top & {}^{l+1} \hat{\Sigma}_M^{l+2:L, l+2:L} \end{pmatrix} \right), \quad (73)$$

where the terms are defined in Eqs. (19), (20), and (35). That means we have to prove that $\hat{m}_n^{l+1} = \hat{\mu}_n^{l+1}$ and similarly for the other terms in Eqs. (69) - (72). Note that this is the point where we need the left indices in order to distinguish e.g. the term ${}^l \hat{\mu}_M^{l+2:L}$ appearing in Eq. (69) from ${}^{l+1} \hat{\mu}_M^{l+2:L}$ appearing in the mean of Eq. (73).

We will exemplarily prove that $\hat{m}_n^{l+1} = \hat{\mu}_n^{l+1}$: Starting from Eq. (68) we have

$$\begin{aligned} \hat{m}_n^{l+1} &= \tilde{\mathcal{K}}_{nM}^{l+1} \left({}^l \hat{\mu}_M^{l+1} + \left({}^l \hat{\Sigma}_{nM}^{l+1, l} \right)^\top \left(\hat{\Sigma}_n^l \right)^{-1} (f_n^l - \hat{\mu}_n^l) \right) \\ &= \tilde{\mu}_n^{l+1} + \tilde{S}_n^{l+1, 1:l-1} \left(\tilde{S}_n^{1:l-1, 1:l-1} \right)^{-1} (f_n^{1:l-1} - \tilde{\mu}_n^{1:l-1}) + \left(\tilde{S}_n^{l+1, l} - \tilde{S}_n^{l+1, 1:l-1} \left(\tilde{S}_n^{1:l-1, 1:l-1} \right)^{-1} \tilde{S}_n^{1:l-1, l} \right) \times \\ &\quad \left(\hat{\Sigma}_n^l \right)^{-1} \left(f_n^l - \tilde{\mu}_n^l - \tilde{S}_n^{l, 1:l-1} \left(\tilde{S}_n^{1:l-1, 1:l-1} \right)^{-1} (f_n^{1:l-1} - \tilde{\mu}_n^{1:l-1}) \right), \end{aligned} \quad (74)$$

where we used the definitions in Eqs. (19) and (35) for the terms $\hat{\cdot}$. Note that these definitions are part of the induction hypothesis. It will soon become clear why we did not substitute $\hat{\Sigma}_n^l$. We furthermore used the definitions in Eqs. (21) and (22) to absorb the $\tilde{\mathcal{K}}$ terms. In the following we are going to write Eq. (74) in a vectorized form and additionally substitute

$$A = \tilde{S}_n^{1:l-1, 1:l-1}, \quad B = \tilde{S}_n^{1:l-1, l}, \quad C = \tilde{S}_n^{l, 1:l-1}, \quad \tilde{D} = \hat{\Sigma}_n^l, \quad (75)$$

The reason for these steps will become clear after two more equations:

$$\hat{m}_n^{l+1} = \tilde{\mu}_n^{l+1} + \begin{pmatrix} \tilde{S}_n^{l+1,1:l-1}A^{-1} - (\tilde{S}_n^{l+1,l} - \tilde{S}_n^{l+1,1:l-1}A^{-1}B)\tilde{D}^{-1}CA^{-1} \\ (\tilde{S}_n^{l+1,l} - \tilde{S}_n^{l+1,1:l-1}A^{-1}B)\tilde{D}^{-1} \end{pmatrix}^\top \begin{pmatrix} f_n^{1:l-1} - \tilde{\mu}_n^{1:l-1} \\ f_n^l - \tilde{\mu}_n^l \end{pmatrix} \quad (76)$$

Going one step further, we recognize this as a vector matrix multiplication,

$$\hat{m}_n^{l+1} = \tilde{\mu}_n^{l+1} + \begin{pmatrix} \tilde{S}_n^{l+1,1:l-1} \\ \tilde{S}_n^{l+1,l} \end{pmatrix}^\top \begin{pmatrix} A^{-1} + A^{-1}B\tilde{D}^{-1}CA^{-1} & -A^{-1}B\tilde{D}^{-1} \\ -\tilde{D}^{-1}CA^{-1} & \tilde{D}^{-1} \end{pmatrix} \begin{pmatrix} f_n^{1:l-1} - \tilde{\mu}_n^{1:l-1} \\ f_n^l - \tilde{\mu}_n^l \end{pmatrix}, \quad (77)$$

where we additionally exploited that A and \tilde{D} are symmetric and that $B^\top = C$. In order to get any further from here we need the block matrix inversion lemma, which states that

$$\begin{pmatrix} A & B \\ C & D \end{pmatrix}^{-1} = \begin{pmatrix} A^{-1} + A^{-1}B\tilde{D}^{-1}CA^{-1} & -A^{-1}B\tilde{D}^{-1} \\ -\tilde{D}^{-1}CA^{-1} & \tilde{D}^{-1} \end{pmatrix}, \quad (78)$$

where $\tilde{D} = D - CA^{-1}B$. Comparing Eqs. (77) and (78) explains why we insisted on vectorising the last few formulas and also our definitions in Eq. (75). Finally, since $\hat{\Sigma}_n^l = \tilde{S}_n^{ll} - \tilde{S}_n^{l,1:l-1}(\tilde{S}_n^{1:l-1,1:l-1})^{-1}\tilde{S}_n^{1:l-1,l}$ [Eq. (20)], we also identify $\tilde{S}_n^{ll} = D$. We can therefore rewrite Eq. (77) by reversing the block matrix inversion and resubstituting the terms in Eq. (75):

$$\begin{aligned} \hat{m}_n^{l+1} &= \tilde{\mu}_n^{l+1} + \begin{pmatrix} \tilde{S}_n^{l+1,1:l-1} \\ \tilde{S}_n^{l+1,l} \end{pmatrix}^\top \begin{pmatrix} \tilde{S}_n^{1:l-1,1:l-1} & \tilde{S}_n^{1:l-1,l} \\ \tilde{S}_n^{l,1:l-1} & \tilde{S}_n^{ll} \end{pmatrix}^{-1} \begin{pmatrix} f_n^{1:l-1} - \tilde{\mu}_n^{1:l-1} \\ f_n^l - \tilde{\mu}_n^l \end{pmatrix} \\ &= \tilde{\mu}_n^{l+1} + \tilde{S}_n^{l+1,1:l}(\tilde{S}_n^{1:l,1:l})^{-1}(f_n^{1:l} - \tilde{\mu}_n^{1:l}). \end{aligned} \quad (79)$$

In the last step we simply rewrote the vectors and the matrix according to the way we defined the submatrix notation. Comparing the final result to Eq. (19), we realize that this is indeed $\hat{\mu}_n^{l+1}$, i.e., the mean term where we substituted $l \rightarrow l + 1$. In exactly the same way, i.e., by reversing the matrix inversion, we can show that the other parameters of the distribution in Eq. (67) indeed coincide with the respective parameters of the distribution in Eq. (73). Since this was the last part that remained to be shown, we finished the proof of Lem. 2. \square

B ELBO

Here we show how to derive the ELBO of the FC DGP, i.e., Eq. (16), which is given by

$$\mathcal{L} = \sum_{n=1}^N \mathbb{E}_{q(f_n^L)} [\log p(y_n | f_n^L)] - \text{KL}[q(f_M) || \prod_{l=1}^L p(f_M^l)]. \quad (80)$$

While this is already done in the supplemental material of Ref. [7], we will do the derivation once again since our notation is different. For convenience we repeat the relevant formulas from the main text, i.e., the general formula for the ELBO [Eq. (4)], the joint DGP prior [Eq. (9)], and the variational family for the DGP [Eq. (10)], which are given by

$$\mathcal{L} = \int q(f_N, f_M) \log \frac{p(y_N, f_N, f_M)}{q(f_N, f_M)} df_N df_M, \quad (81)$$

$$p(y_N, f_N, f_M) = p(y_N | f_N^L) \prod_{l=1}^L p(f_N^l | f_M^l; f_N^{l-1}) p(f_M^l), \quad (82)$$

$$q(f_N, f_M) = q(f_M) \prod_{l=1}^L p(f_N^l | f_M^l; f_N^{l-1}), \quad (83)$$

respectively. By only using the general form of the distributions, and exploiting that we assumed iid noise, i.e., $p(y_N|f_N^L) = \prod_{n=1}^N p(y_n|f_n^L)$, we can get from Eq. (81) to Eq. (80):

$$\mathcal{L} = \int q(f_N, f_M) \log \frac{p(y_N, f_N, f_M)}{q(f_N, f_M)} df_N df_M = \int q(f_N, f_M) \log \frac{p(y_N|f_N^L) \prod_{l=1}^L p(f_M^l)}{q(f_M)} df_N df_M \quad (84)$$

$$= \int q(f_N, f_M) \log p(y_N|f_N^L) df_N df_M + \int q(f_N, f_M) \log \frac{\prod_{l=1}^L p(f_M^l)}{q(f_M)} df_N df_M, \quad (85)$$

$$= \int q(f_N, f_M) \log \prod_{n=1}^N p(y_n|f_n^L) df_N df_M + \int q(f_M) \log \frac{\prod_{l=1}^L p(f_M^l)}{q(f_M)} df_M, \quad (86)$$

$$= \sum_{n=1}^N \int q(f_n^L) \log p(y_n|f_n^L) df_n^L - \text{KL}[q(f_M) \| \prod_{l=1}^L p(f_M^l)]. \quad (87)$$

In the last step we introduced $q(f_n^L)$ as simply summarising all remaining terms in the first integral, hence

$$q(f_n^L) = \int q(f_N, f_M) df_M \prod_{n' \neq n} df_{n'}^L \prod_{l=1}^{L-1} df_N^l. \quad (88)$$

C Marginalisation of (most) latent layer outputs

Here we show how to get from the general form of $q(f_n^L)$ given in Eq. (88) to the starting point of our induction proof [Eq. (23)], where all the latent outputs $f_{n'}^l$ are integrated out for all layers l and for all samples $n' \neq n$:

$$q(f_n^L) = \int \left[\int q(f_M) \prod_{l=1}^L p(f_n^l | f_M^l; f_n^{l-1}) df_M \right] df_n^1 \cdots df_n^{L-1}. \quad (89)$$

While this is already shown in Remark 2 in Ref. [7] (note that the indices there are not correct), we will provide a bit more detail here and we can also nicely point out where the difference in the formulas for $q(f_n^L)$ arises from. For convenience the relevant formulas are repeated below:

$$q(f_N, f_M) = q(f_M) \prod_{l=1}^L p(f_N^l | f_M^l; f_N^{l-1}), \quad p(f_N^l | f_M^l; f_N^{l-1}) = \mathcal{N}\left(f_N^l \mid \tilde{\mathcal{K}}_{NM}^l f_M^l, \tilde{\mathcal{K}}_{NN}^l\right), \quad (90)$$

where $\tilde{\mathcal{K}}_{NM}^l = \mathcal{K}_{NM}^l (\mathcal{K}_{MM}^l)^{-1}$ and $\tilde{\mathcal{K}}_{NN}^l = \mathcal{K}_{NN}^l - \mathcal{K}_{NM}^l (\mathcal{K}_{MM}^l)^{-1} \mathcal{K}_{MN}^l$.

We will start by explicitly writing out Eq. (88) and changing the order of integration:

$$q(f_n^L) = \int q(f_M) \left[\int \prod_{l=1}^L p(f_N^l | f_M^l; f_N^{l-1}) \prod_{n' \neq n} df_{n'}^L \prod_{l=1}^{L-1} df_N^l \right] df_M. \quad (91)$$

In the following we will only be concerned with the inner integral of the previous equation, which can also be written as

$$\int \left(\int p(f_N^L | f_M^L; f_N^{L-1}) \prod_{n' \neq n} df_{n'}^L \right) \prod_{l=1}^{L-1} p(f_N^l | f_M^l; f_N^{l-1}) df_N^l. \quad (92)$$

Here, the inner integral can be solved by exploiting the nice marginalisation property of multivariate Gaussians,

$$\int p(f_N^L | f_M^L; f_N^{L-1}) \prod_{n' \neq n} df_{n'}^L = \int \mathcal{N}\left(f_N^L \mid \tilde{\mathcal{K}}_{NM}^L (f_N^{L-1}) f_M^L, \tilde{\mathcal{K}}_{NN}^L (f_N^{L-1})\right) \prod_{n' \neq n} df_{n'}^L \quad (93)$$

$$= \mathcal{N}\left(f_n^L \mid \tilde{\mathcal{K}}_{nM}^L (f_N^{L-1}) f_M^L, \tilde{\mathcal{K}}_{nn}^L (f_N^{L-1})\right), \quad (94)$$

where we explicitly marked the dependence of the $\tilde{\mathcal{K}}^l$ terms on the outputs f_N^{L-1} . While the $\tilde{\mathcal{K}}_{nM}^l$ could in principle still depend on all the outputs of the previous layer, we see from their definitions after Eq. (90) that they infact only depend on the marginals f_n^{L-1} and that therefore

$$\mathcal{N}\left(f_n^L \mid \tilde{\mathcal{K}}_{nM}^L(f_N^{L-1})f_M^L, \tilde{\mathcal{K}}_{nn}^L(f_N^{L-1})\right) = \mathcal{N}\left(f_n^L \mid \tilde{\mathcal{K}}_{nM}^L(f_n^{L-1})f_M^L, \tilde{\mathcal{K}}_{nn}^L(f_n^{L-1})\right) = p(f_n^L \mid f_M^L; f_n^{L-1}). \quad (95)$$

Putting the last two equations together results in

$$\int p(f_N^L \mid f_M^L; f_N^{L-1}) \prod_{n' \neq n} df_{n'}^L = p(f_n^L \mid f_M^L; f_n^{L-1}). \quad (96)$$

We can continue with integrating out the f_N^l in Eq. (92) in the same fashion (noting at every layer that we can not marginalise out f_n^l as those are inputs to kernels), arriving at

$$\int \prod_{l=1}^L p(f_N^l \mid f_M^l; f_N^{l-1}) \prod_{n' \neq n} df_{n'}^L \prod_{l=1}^{L-1} df_N^l = \int \prod_{l=1}^L p(f_n^l \mid f_M^l; f_n^{l-1}) df_n^1 \cdots df_n^{L-1}. \quad (97)$$

Plugging this back into Eq. (91) and changing the order of integration once again, yields

$$q(f_n^L) = \int \left[\int q(f_M) \prod_{l=1}^L p(f_n^l \mid f_M^l; f_n^{l-1}) df_M \right] df_n^1 \cdots df_n^{L-1}, \quad (98)$$

which is exactly Eq. (89), the result that we set out to show.

C.1 Difference between mean-field and fully-coupled

From this equation it is also possible to see why a proof as in Appx. A was not necessary for the MF DGP. This is due to the form of the variational posterior over the inducing outputs, given by

$$q(f_M) = \begin{cases} \mathcal{N}(f_M \mid \mu_M, S_M) & \text{for the FC DGP,} \\ \prod_{l=1}^L \prod_{t=1}^{T_l} \mathcal{N}(f_M^{l,t} \mid \mu_M^{l,t}, S_M^{l,t}) & \text{for the MF DGP.} \end{cases} \quad (99)$$

Using $q(f_M)$ from the MF DGP, which can also be written as $q(f_M) = \prod_{l=1}^L q(f_M^l)$, the inner integral in Eq. (98) can be rewritten as the product of l integrals,

$$\int q(f_M) \prod_{l=1}^L p(f_n^l \mid f_M^l; f_n^{l-1}) df_M = \prod_{l=1}^L \int q(f_M^l) p(f_n^l \mid f_M^l; f_n^{l-1}) df_M^l, \quad (100)$$

each being a standard integral in Gaussian calculus and the resulting formulas are given in Eqs. (13) and (14). In contrast, a fully coupled multivariate Gaussian can not be written as such a product, which is why the rather straightforward solution presented above is not possible in our case and the proof in Appx. A is needed.

D Linear algebra to speed up the code

In this section we provide some guidance through the linear algebra that is exploited in our code to speed up or vectorise calculations. We will focus only on the most expensive terms, i.e., the off-diagonal covariance term $\tilde{S}_n^{l,1:l-1}$ and how to deal with $\left(\tilde{S}_n^{1:l-1,1:l-1}\right)^{-1}$, which are both needed to calculate $\hat{\mu}_n^l$ and $\hat{\Sigma}_n^l$ in Eqs. (101) and (102), respectively. First, we show how to deal with the FC DGP and afterwards how the sparsity of S_M for the STAR DGP can be used. The linear algebra that can be exploited for all the other terms, e.g. the KL-divergence, will be provided along with the code. Our implementation is in GPflow [23] which provides all the functionalities that are necessary to deal with GPs in Tensorflow [24].

Before we start we will repeat some formulas for convenience:

$$\hat{\mu}_n^l = \tilde{\mu}_n^l + \tilde{S}_n^{l,1:l-1} \left(\tilde{S}_n^{1:l-1,1:l-1} \right)^{-1} (f_n^{1:l-1} - \tilde{\mu}_n^{1:l-1}), \quad (101)$$

$$\hat{\Sigma}_n^l = \tilde{S}_n^l - \tilde{S}_n^{l,1:l-1} \left(\tilde{S}_n^{1:l-1,1:l-1} \right)^{-1} \tilde{S}_n^{1:l-1,l}, \quad (102)$$

$$\tilde{S}_n^{ll'} = \left(\tilde{\mathcal{K}}_{Mn}^l \right)^\top S_M^{ll'} \tilde{\mathcal{K}}_{Mn}^{l'}, \quad \text{if } l \neq l'. \quad (103)$$

Additionally, here is a more explicit definition of our notation of the covariance matrix S_M :

$$S_M = \begin{pmatrix} S_M^{11} & \cdots & S_M^{1L} \\ \vdots & \ddots & \vdots \\ S_M^{L1} & \cdots & S_M^{LL} \end{pmatrix}, \quad S_M^{ll'} = \begin{pmatrix} \left(S_M^{ll'} \right)_{11} & \cdots & \left(S_M^{ll'} \right)_{1T_{l'}} \\ \vdots & \ddots & \vdots \\ \left(S_M^{ll'} \right)_{T_l 1} & \cdots & \left(S_M^{ll'} \right)_{T_l T_{l'}} \end{pmatrix}, \quad (104)$$

where S_M , $S_M^{ll'}$, and $\left(S_M^{ll'} \right)_{tt'}$ are matrices of size $MT \times MT$ (where $T = \sum_{l=1}^L T_l$), $MT_l \times MT_{l'}$, and $M \times M$, which store the covariances of the inducing outputs between all inducing points, only those between layer l and l' , and only those between the t -th task in layer l and the t' -th task in layer l' , respectively. In order to ensure that S_M is a valid covariance matrix (positive definite) we will numerically only work with its Cholesky decomposition L_S (s.t. $S_M = L_S L_S^\top$), which is a lower triangular matrix. Wherever possible we will want to avoid actually computing S_M and instead calculate all quantities from L_S directly.

D.1 Fully coupled DGP

Off-diagonal covariance terms The terms

$$\tilde{S}_n^{l,1:l-1} = \begin{pmatrix} \tilde{S}_n^{l1} & \tilde{S}_n^{l2} & \cdots & \tilde{S}_n^{l,l-1} \end{pmatrix}, \quad (105)$$

which are of size $T_l \times \sum_{l'=1}^{l-1} T_{l'}$, have to be calculated for $l = 1, \dots, L$ and for $n = 1, \dots, N$. As the number of layers L is in practice rather small, we will calculate all the individual matrices $\tilde{S}_n^{ll'}$ in a loop and concatenate them at the end, while we want to avoid a loop over N . Using Eq. (103) and that $\tilde{\mathcal{K}}_{Mn}^l = \mathbb{I}_{T_l} \otimes \tilde{K}_{Mn}^l$, we see that (for an example with $T_l, T_{l'} = 2$)

$$\tilde{S}_n^{ll'} = \begin{pmatrix} \left(\tilde{K}_{Mn}^l \right)^\top (S_M^{ll'})_{11} \tilde{K}_{Mn}^{l'} & \left(\tilde{K}_{Mn}^l \right)^\top (S_M^{ll'})_{12} \tilde{K}_{Mn}^{l'} \\ \left(\tilde{K}_{Mn}^l \right)^\top (S_M^{ll'})_{21} \tilde{K}_{Mn}^{l'} & \left(\tilde{K}_{Mn}^l \right)^\top (S_M^{ll'})_{22} \tilde{K}_{Mn}^{l'} \end{pmatrix}. \quad (106)$$

Writing $\tilde{S}_n^{ll'}$ in this way has two advantages: Firstly, actually performing the multiplication $\tilde{\mathcal{K}}_{Mn}^l S_M^{ll'} \tilde{\mathcal{K}}_{Mn}^{l'}$ is extremely inefficient as the $\tilde{\mathcal{K}}_{Mn}^l$ are block diagonal, which we resolved in this formulation. Secondly, we note that exactly the same operation, i.e., multiplying from left and right by $\left(\tilde{K}_{Mn}^l \right)^\top$ and $\tilde{K}_{Mn}^{l'}$, respectively, has to be performed on all $T_l T_{l'}$ blocks of size $M \times M$. This can be exploited since tensorflow has an inbuilt batch mode for most of its matrix operations. In the following we will first show how the relevant block $S_M^{ll'}$ can be efficiently obtained and afterwards show how to deal with the batch matrix multiplication for all $n = 1, \dots, N$.

Let us consider an example with three layers ($L = 3$), the resulting covariance matrix and its Cholesky decomposition:

$$S_M = \begin{pmatrix} S_M^{11} & S_M^{12} & S_M^{13} \\ S_M^{21} & S_M^{22} & S_M^{23} \\ S_M^{31} & S_M^{32} & S_M^{33} \end{pmatrix} = L_S L_S^\top = \begin{pmatrix} L_S^{11} & 0 & 0 \\ L_S^{21} & L_S^{22} & 0 \\ L_S^{31} & L_S^{32} & L_S^{33} \end{pmatrix} \begin{pmatrix} (L_S^{11})^\top & (L_S^{21})^\top & (L_S^{31})^\top \\ 0 & (L_S^{22})^\top & (L_S^{32})^\top \\ 0 & 0 & (L_S^{33})^\top \end{pmatrix}. \quad (107)$$

From this we can read off formulas for the blocks of S_M , e.g., $S_M^{32} = (L_S^{31} \ L_S^{32}) (L_S^{21} \ L_S^{22})^\top$, which in general can be written as

$$S_M^{ll'} = L_S^{l,1:l'} \left(L_S^{l',1:l'} \right)^\top, \quad (108)$$

where we exploited that we only need $S_M^{l'}$ for $l' < l$ (the formula above is not valid for $l' \geq l$). In this way we avoided calculating unnecessary matrix multiplications involving zero blocks.

Avoiding the loop over N requires a bit more linear algebra: For this we note that e.g. the element $(\tilde{S}_n^l)_{11}$ can be seen as the n -th diagonal element of the $N \times N$ matrix $(\tilde{K}_{MN}^l)^\top (S_M^{l'})_{11} \tilde{K}_{MN}^{l'}$. Fully calculating this matrix is obviously very inefficient as we only need its diagonal elements. For this we use that, generally, for $q \times p$ matrices A , C^\top and $q \times q$ matrices B

$$\text{diag}(C^\top BA) = \text{column_sum}(C^\top \odot BA), \quad (109)$$

where \odot denotes the elementwise matrix product. The formula can easily be proved by explicitly writing the matrix products as sums and comparing terms on both sides. Using this on all the blocks of $\tilde{S}_n^{l'}$ in Eq. (106) in a batched form and reordering the obtained terms afterwards requires some reshaping, which is explained in the code.

The most expensive calculations for this term are obtaining $S_M^{l'}$ [Eq. (108)], which is $\mathcal{O}(M^3 T_l T_{l'} \sum_{l''=1}^{l'} T_{l''})$ and the multiplication of e.g. $(S_M^{l'})_{11} \tilde{K}_{MN}^{l'}$ which has to be done for all $T_l T_{l'}$ blocks of $S_M^{l'}$ and is therefore $\mathcal{O}(NM^2 T_l T_{l'})$. Both of these operations have to be performed for all $l' = 1, \dots, l-1$ in Eq. (105) and also for all layers $l = 1, \dots, L$. The total computational cost of this term is therefore $\mathcal{O}(M^3 \sum_{l=1}^L T_l \sum_{l'=1}^{l-1} T_{l'} \sum_{l''=1}^{l'} T_{l''} + NM^2 \sum_{l=1}^L T_l \sum_{l'=1}^{l-1} T_{l'})$.

Dealing with the inverse covariance terms First of all, we will never actually calculate $(\tilde{S}_n^{1:l-1,1:l-1})^{-1}$. We will only use (and update) the lower triangular Cholesky decomposition $L_{S_n}^{1:l-1,1:l-1}$ defined by

$$L_{S_n}^{1:l-1,1:l-1} \left(L_{S_n}^{1:l-1,1:l-1} \right)^\top = \tilde{S}_n^{1:l-1,1:l-1}. \quad (110)$$

This can be done since the inverse term only ever appears in the product $\tilde{S}_n^{l,1:l-1} \left(\tilde{S}_n^{1:l-1,1:l-1} \right)^{-1}$, whose transpose can be efficiently obtained via the solution of two triangular systems (which is implemented as `cholesky_solve` in `tensorflow`). For this we obviously need the Cholesky decomposition first. We will point out how this can be efficiently calculated in the following, taking the calculations for the second layer as an example:

After having calculated $\hat{\mu}_n^2$ and $\hat{\Sigma}_n^2$ [Eqs. (101) and (102), respectively] we necessarily still have the quantities $\tilde{L}_{S_n}^{11}$ (passed on from the first layer calculations), \tilde{S}_n^{12} , and \tilde{S}_n^{22} in memory. Note that we therefore can completely build the block matrix $\tilde{S}_n^{1:2,1:2}$ as

$$\tilde{S}_n^{1:2,1:2} = \begin{pmatrix} \tilde{L}_{S_n}^{11} \left(\tilde{L}_{S_n}^{11} \right)^\top & \tilde{S}_n^{12} \\ \left(\tilde{S}_n^{12} \right)^\top & \tilde{S}_n^{22} \end{pmatrix} \quad (111)$$

from which we could in principle calculate the Cholesky factor directly. A more efficient way is to assume a general block matrix form for the Cholesky factor,

$$\tilde{L}_{S_n}^{1:2,1:2} = \begin{pmatrix} A & 0 \\ B & C \end{pmatrix}, \quad (112)$$

and then by using Eq. (110) and comparing the terms to Eq. (111) finding formulas for the unknown terms and solve them. These formulas are given by

$$AA^\top = \tilde{L}_{S_n}^{11} \left(\tilde{L}_{S_n}^{11} \right)^\top, \quad (113)$$

$$AB^\top = \tilde{S}_n^{12}, \quad (114)$$

$$BB^\top + CC^\top = \tilde{S}_n^{22}. \quad (115)$$

From Eq. (113) we recognize $A = \tilde{L}_{S_n}^{11}$. Next, we can use this and Eq. (114) to find B^\top as the solution of the (triangular) system $\tilde{L}_{S_n}^{11} B^\top = \tilde{S}_n^{12}$. The last step is then to obtain C from the Cholesky decomposition of the matrix $\tilde{S}_n^{22} - BB^\top$, where we used Eq. (115). Note that while we still have to do a Cholesky decomposition, the matrix that

has to be decomposed is (especially for large l) considerably smaller than the full matrix $\tilde{S}_n^{1:2,1:2}$ and the computation therefore much faster. For general l we simply have to substitute $\tilde{L}_{S_n}^{11} \rightarrow \tilde{L}_{S_n}^{1:l-1,1:l-1}$, $\tilde{S}_n^{12} \rightarrow \tilde{S}_n^{1:l-1,l}$, and $\tilde{S}_n^{22} \rightarrow \tilde{S}_n^{ll}$, the rest stays the same. Plugging the obtained results for A , B , and C in Eq. (112) yields the required "updated" Cholesky factor that needs to be passed on for the calculations in the next layer.

Solving the three equations (113) - (115) for layer l requires $\mathcal{O}(N(T_l^2 \sum_{l'=1}^{l-1} T_{l'} + T_l(\sum_{l'=1}^{l-1} T_{l'})^2 + T_l^3))$ computation time. Doing so for all layers (note that we do not have to do this for the last layer) is therefore $\mathcal{O}(N \sum_{l=1}^{L-1} (T_l^2 \sum_{l'=1}^{l-1} T_{l'} + T_l(\sum_{l'=1}^{l-1} T_{l'})^2 + T_l^3))$

Computational costs Since these were the most expensive terms for the FC DGP, the overall computational cost for evaluating the ELBO is therefore

$$\mathcal{O} \left(N \sum_{l=1}^L \left[M^2 T_l \sum_{l'=1}^{l-1} T_{l'} + T_l^2 \sum_{l'=1}^{l-1} T_{l'} + T_l \left(\sum_{l'=1}^{l-1} T_{l'} \right)^2 + T_l^3 + \frac{M^3}{N} T_l \sum_{l'=1}^{l-1} T_{l'} \sum_{l''=1}^{l'} T_{l''} \right] \right). \quad (116)$$

In order to get a better grasp at this we will take an example architecture with L layers and the same number $T_l = \tau$ of GPs per layer except for the last layer in which there is only one GP ($T_L = 1$). In such a case the computational cost simplifies to

$$\mathcal{O}(NM^2\tau^2L^2 + N\tau^3L^3 + M^3\tau^3L^3), \quad (117)$$

where we only kept the highest order terms.

D.2 Stripes-and-Arrow DGP

In the following we will briefly sketch the computational savings that can be achieved for the two terms discussed in the previous section, when the restricted covariance of the STAR DGP is used. Note that in this case the architecture necessarily needs to be the one described in the example given in the previous paragraph. The (potential) non-zero $M \times M$ blocks of the covariance matrix can be described by $\left(S_M^{ll'} \right)_{tt'}$, where $t = t'$ (this captures the terms also present in the MF DGP plus the diagonal stripes) or $l = L$ or $l' = L$ (this captures the two sides of the arrowhead). It is easy to see that this form directly translates to the Cholesky decomposition which we will exploit in the next section: The lower diagonal L_S has (potential) non-zero $M \times M$ blocks $\left(L_S^{ll'} \right)_{tt'}$, only if $l \geq l'$ (lower diagonal) and if $t = t'$ (diagonal and stripes) or $l = L$ (arrowhead).

Computing the covariance matrix from its Cholesky decomposition We will start by describing how the relevant terms of S_M can be obtained from our chosen sparse representation of L_S , where we summarise the non-zero terms in three arrays, $\text{diag } L_S$, $\text{stripes } L_S$, and $\text{arrow } L_S$. The array $\text{diag } L_S$ contains the $\tau(L-1) + 1$ lower diagonal $M \times M$ blocks on the diagonal of L_S , where we access the t -th block in the l -th layer, i.e., $\left(L_S^{ll} \right)_{tt}$, by $\text{diag } L_S^{l,t}$. The array $\text{stripes } L_S$ contains the $\tau \sum_{k=1}^{L-2} k = \frac{\tau}{2}(L-2)(L-1)$ blocks of size $M \times M$, which form the diagonal stripes of L_S , where we access $\left(L_S^{ll'} \right)_{tt}$ (where $L > l > l'$) by $\text{stripes } L_S^{l,l',t}$. The remaining $\tau(L-1)$ blocks of size $M \times M$ of the arrowhead are contained in $\text{arrow } L_S$, where we access $\left(L_S^{ll} \right)_{1t}$ as $\text{arrow } L_S^{l,t}$. See also Fig. 1 for a depiction of the covariance matrix.

The different terms of S_M can then be obtained as listed below:

i) Diagonal terms $\left(S_M^{ll} \right)_{tt}$ with $l < L$:

$$\left(S_M^{ll} \right)_{tt} = \text{diag } L_S^{l,t} \left(\text{diag } L_S^{l,t} \right)^\top + \sum_{l'=1}^{l-1} \text{stripes } L_S^{l,l',t} \left(\text{stripes } L_S^{l,l',t} \right)^\top \quad (118)$$

ii) Diagonal term $\left(S_M^{LL} \right)_{11}$:

$$\left(S_M^{LL} \right)_{11} = \text{diag } L_S^{L,1} \left(\text{diag } L_S^{L,1} \right)^\top + \sum_{l=1}^{L-1} \sum_{t=1}^{\tau} \text{arrow } L_S^{l,t} \left(\text{arrow } L_S^{l,t} \right)^\top \quad (119)$$

iii) Stripe terms $\left(S_M^{ll'}\right)_{tt}$ with $L > l > l'$ ($l < l'$ obtained via transposing):

$$\left(S_M^{ll'}\right)_{tt} = \text{stripes } L_S^{l,l',t} \left(\text{diag } L_S^{l',t}\right)^\top + \sum_{l''=1}^{l'-1} \text{stripe } L_S^{l,l'',t} \left(\text{stripes } L_S^{l',l'',t}\right)^\top \quad (120)$$

iv) Arrow terms $\left(S_M^{Ll}\right)_{1t}$:

$$\left(S_M^{Ll}\right)_{1t} = \text{arrow } L_S^{l,t} \left(\text{diag } L_S^{l,t}\right)^\top + \sum_{l'=1}^{l-1} \text{arrow } L_S^{l',t} \left(\text{stripes } L_S^{l,l',t}\right)^\top \quad (121)$$

The vectorisation of these equations can be seen in the code. The stripe terms are the most expensive to compute since an individual term has computational cost $\mathcal{O}(M^3 l')$ which has to be done for $l = 2, \dots, L-1$ and for $l' = 1, \dots, l-1$ and for all $t = 1, \dots, \tau$. Therefore calculating all stripe terms is $\mathcal{O}(M^3 L^3 \tau)$ (where we only kept the highest order term).

Off-diagonal covariance terms As before with the FC DGP, the off-diagonal covariance terms $\tilde{S}_n^{ll'}$ will also be the most expensive to compute. From the general formula in Eq. (103) it is easy to see that $\left(\tilde{S}_n^{ll'}\right)_{tt'}$ is only non-zero, if the corresponding $\left(S_M^{ll'}\right)_{tt'}$ are non-zero. We showed in the previous paragraph how those can be calculated, so the only step that remains to be done is the equivalent of Eq. (106), where again Eq. (109) can be used.

Doing this for an individual $M \times M$ block can be done in $\mathcal{O}(NM^2)$ time. Since we have to do this for all $\mathcal{O}(\tau L^2)$ blocks, the total computational cost for the off-diagonal covariance terms is $\mathcal{O}(NM^2 \tau L^2)$.

Dealing with the inverse covariance terms For calculating (or updating) the Cholesky decomposition of $\tilde{S}_n^{1:l-1, 1:l-1}$ we could in principle use similar ideas as we used above for calculating S_M (since both have the same sparsity pattern). But as we saw in the previous section, this term only incurs computational costs of $\mathcal{O}(N\tau^3 L^3)$ even for the FC DGP, which is for our settings always the least expensive term. We therefore simply reuse the algorithm described in the previous section to deal with this term and live with the resulting computational costs.

Computational costs The total computational costs for calculating the ELBO for the STAR DGP are therefore

$$\mathcal{O}(NM^2 \tau L^2 + N\tau^3 L^3 + M^3 \tau L^3). \quad (122)$$

E Additional experimental details

In the following, we describe the experimental details necessary to reproduce the results:

- **Data Normalization** Normalization of inputs and outputs to zero mean and unit variance based on the training data.
- **Inducing Inputs** $M = 128$ inducing inputs initialized with k-means.
- **DGP architecture** $L = 3$ hidden layers with $\tau = 5$ latent GPs each and principal components of the training data as mean function.
- **Likelihood** Gaussian likelihood with initial variance $\sigma_0^2 = 0.01$.
- **Kernel** RBF kernel with automatic relevance determination (initial lengthscale $l_0 = 1$, initial variance $\sigma_0^2 = 1$).
- **Optimizer** Adam Optimizer (number of iterations $nIter = 20,000$, mini-batch size $mbs = 512$) with exponentially decaying learning rate (learning rate $lr = 0.005$, steps $s = 1000$, rate $r = 0.98$).

Dataset (N,D)	SGP	SGHMC DGP			MF DGP		STAR DGP	
	L1	L1	L2	L3	L2	L3	L2	L3
boston (506,13)	-2.58(0.10)	-2.75(0.18)	-2.51(0.07)	-2.53(0.09)	-2.43(0.05)	-2.48(0.06)	-2.47(0.08)	-2.43(0.05)
energy (768, 8)	-0.71(0.03)	-1.16(0.44)	-0.37(0.12)	-0.34(0.11)	-0.73(0.02)	-0.75(0.02)	-0.75(0.02)	-0.75(0.02)
concrete (1030, 8)	-3.09(0.02)	-3.50(0.34)	-2.89(0.06)	-2.88(0.06)	-3.06(0.03)	-3.09(0.02)	-3.04(0.02)	-3.05(0.02)
wine red (1599,11)	-0.88(0.01)	-0.90(0.03)	-0.81(0.03)	-0.80(0.07)	-0.89(0.01)	-0.89(0.01)	-0.88(0.01)	-0.88(0.01)
kin8nm (8192, 8)	1.05(0.01)	1.14(0.01)	1.38(0.01)	1.25(0.14)	1.30(0.01)	1.31(0.01)	1.28(0.01)	1.29(0.01)
power (9568, 4)	-2.78(0.01)	-2.75(0.02)	-2.68(0.02)	-2.65(0.02)	-2.77(0.01)	-2.76(0.01)	-2.77(0.01)	-2.77(0.01)
naval (11934,16)	7.56(0.09)	7.77(0.04)	7.32(0.02)	6.89(0.43)	7.11(0.11)	7.05(0.09)	7.06(0.08)	6.25(0.31)
protein (45730, 9)	-2.91(0.00)	-2.76(0.00)	-2.64(0.01)	-2.58(0.01)	-2.83(0.00)	-2.79(0.00)	-2.83(0.00)	-2.80(0.00)

Table S2: **Interpolation behavior on UCI benchmark datasets.** We report test log-likelihoods (the larger, the better) for various methods. where L denotes the number of layers. We randomly split the data into train and test sets using a ratio of 90:10. Standard errors are obtained by repeating the experiment 10 times. We marked all methods in bold that performed better or as good as the standard sparse GP.

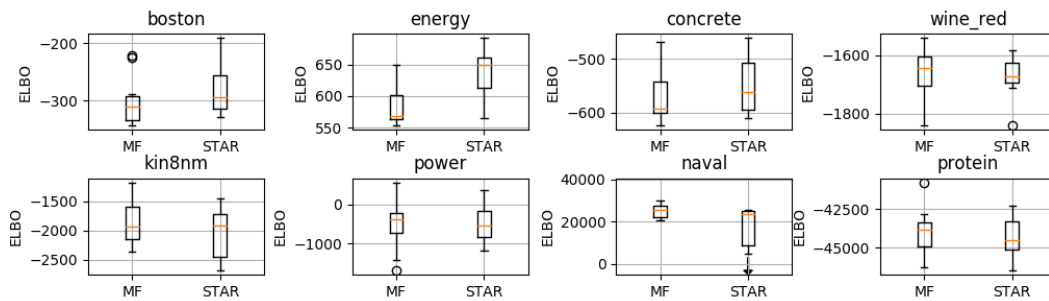


Figure S4: **ELBO comparison.** We show boxplots of the ELBOs that correspond to the interpolation setting reported in Tab. S2 for all datasets and for 10 random splits, comparing the three layer versions of MF DGP and our STAR DGP. Our method seems to work slightly better for the first three datasets, while the MF DGP works better on *naval* and there is no significant difference on the other datasets. For *naval* we observed convergence difficulties in two runs for the STAR DGP, where the ELBOs are not plotted in the figure (indicated by the arrow).

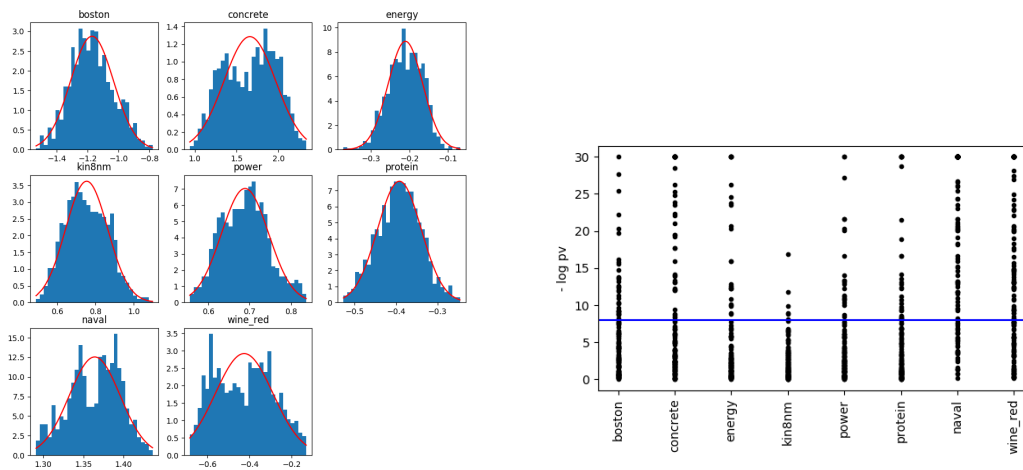


Figure S5: **Convergence of SGHMC.** Left: Distribution over MC samples from a randomly chosen inducing output of a DGP with a single layer, equivalent to a SGP. The red line indicates a Normal distribution fitted to the data. Right: For each inducing output, we computed a p-value if its MC samples are normally distributed. The blue line shows the Bonferroni corrected significance threshold $\alpha = 10^{-5}$.